AD_____

Award Number: W81XWH-04-1-0023

TITLE: MR Imaging Based Treatment Planning for Radiotherapy of Prostate Cancer

PRINCIPAL INVESTIGATOR: Lili Chen, Ph.D.

CONTRACTING ORGANIZATION: Fox Chase Cancer Center
Philadelphia, Pennsylvania 19111

REPORT DATE: February 2005

TYPE OF REPORT: Annual

PREPARED FOR: U.S. Army Medical Research and Materiel Command
Fort Detrick, Maryland 21702-5012

REPORT DOCUMENTATION PAGE

Form Approved
OMB No. 074-0188

1. AGENCY USE ONLY (Leave blank)	2. REPORT DATE	3. REPORT TYPE AND DATES COVERED
	February 2005	Annual (1 Feb 04 - 31 Jan 05)

4. TITLE AND SUBTITLE
MR Imaging Based Treatment Planning for Radiotherapy of Prostate Cancer

5. FUNDING NUMBERS
W81XWH-04-1-0023

6. AUTHOR(S)
Lili Chen, Ph.D.

7. PERFORMING ORGANIZATION NAME(S) AND ADDRESS(ES)
Fox Chase Cancer Center
Philadelphia, Pennsylvania 19111

E-Mail: Lili.Chen@fccc.edu

8. PERFORMING ORGANIZATION REPORT NUMBER

9. SPONSORING / MONITORING AGENCY NAME(S) AND ADDRESS(ES)
U.S. Army Medical Research and Materiel Command
Fort Detrick, Maryland 21702-5012

10. SPONSORING / MONITORING AGENCY REPORT NUMBER

11. SUPPLEMENTARY NOTES

12a. DISTRIBUTION / AVAILABILITY STATEMENT
Approved for Public Release; Distribution Unlimited

12b. DISTRIBUTION CODE

13. ABSTRACT (Maximum 200 Words)

This work is aimed at MRI-based treatment planning for radiation therapy. The tasks for the first year include (a) quantify the effect of MRI distortion on target delineation and treatment planning dose calculation; (b) validate and improve gradient distortion correction for MRI-based treatment planning, (c) investigate the effect of intra-fraction prostate motion and (d) investigate the accuracy of a stereotactic body frame for patient immobilization. We have confirmed that treatment planning dose calculations using MRI-derived homogenous geometry are adequate for patient sizes within 38 cm using the GDC software. We have investigated the effect of MRI residual distortion after GDC on IMRT treatment planning and dosimetry accuracy. Our results showed that the residual distortion errors are < 1 cm, which will have a negligible clinical effect for > 90% of the prostate patients whose lateral dimensions are <40 cm. We have validated the residual distortions and developed computer software to reduce them using point-by point corrections for large patients (up to 42 cm). We have performed studies on the effect of intra-fraction prostate motion using MR cine images and we also have been evaluating the accuracy of a stereotactic body frame for patient immobilization using MRI.

14. SUBJECT TERMS	15. NUMBER OF PAGES
MR-based treatment planning, Dosimetry, Radiotherapy	37
	16. PRICE CODE

17. SECURITY CLASSIFICATION OF REPORT	18. SECURITY CLASSIFICATION OF THIS PAGE	19. SECURITY CLASSIFICATION OF ABSTRACT	20. LIMITATION OF ABSTRACT
Unclassified	Unclassified	Unclassified	Unlimited

Table of Contents

Introduction

This project is aimed at exploring MR imaging based treatment planning for radiotherapy of prostate cancer. We have proposed to work on the first task for the first research year. The tasks include (1) to quantify the effect of MRI distortion on target delineation and treatment planning dose calculation; (2) to validate and improve gradient distortion correction for MRI-based treatment planning; (3) to investigate the effect of intra-fraction prostate motion and (4) to investigate the accuracy of a stereotactic body frame for patient immobilization. In the following we describe our work for the first year.

Body

In this annual report we report on the research accomplishments associated with the tasks outlined in the approved "Statement of Work" task 1 between Feb. 1, 2004 and Feb. 28, 2005. We will provide detailed information below for the results in the first year.

Task 1. Investigate target delineation, localization and patient immobilization using MRI

Quantify the effect of MRI distortion on target delineation and treatment planning dose calculation

During this period, we have focused on investigating the effect of MRI distortion on target delineation and treatment planning dose calculation. Two papers entitled "MRI-based treatment planning for radiotherapy: Dosimetric verification for prostate IMRT" and "Dosimetric evaluation of MRI-based treatment planning for prostate cancer" were published in Int. J. Radiat. Oncol. Biol. Phys. and Physics in Medicine and Biology respectively (Chen et al 2004a, 2004b). We summarize the results and conclusions of these studies as follows.

1) We have studied the use of MRI-based treatment planning for prostate cancer and to verify the dosimetry accuracy of its clinical implementation using a commercial treatment planning system. The AcQPlan system Version 5 was used for the study, which is capable of performing dose calculation on both CT and MRI. A four field 3D conformal planning technique was used for the study. First, we verified the dosimetry accuracy of using homogeneous geometry for prostate planning. This was done by calculating dose distributions using the distortion-free CT data with and without heterogeneity correction (equivalent TAR), respectively. As a result, two treatment plans were generated for each patient with the same treatment parameters (i.e., energy, gantry angle, block shape and size, and dose prescription). Second, we evaluated the dosimetry accuracy between CT-based and MRI-based dose calculation. This was achieved by calculating dose distributions using both CT and MRI data without heterogeneity correction (i.e., using homogeneous geometry defined by the patient external contour). The same MUs obtained from CT-based plans were directly used in MRI-based plans so that the effects of residual MRI distortions on external contours and the differences in internal structure volumes between CT and MRI can be quantified. The plans were evaluated based on isodose distributions and dose volume histograms (DVHs) for the target and the critical structures. Based on the DVHs, doses were reported at 95% of the planned treatment volume (PTV), D95, for the prostate, at 35% (D35) and 17% (D17) of the rectum volume, and at 50% (D50) and 25% (D25) of the bladder volume. These dose points were chosen based on our current clinical acceptance criteria for prostate cancer treatments. Our results confirmed that treatment planning

dose calculations using MRI-derived homogenous geometry are adequate for patient sizes within 38 cm after MR image distortion is corrected using the GDC software (Chen et al 2004b).

2) We have investigated the effect of MRI residual distortion after GDC on IMRT treatment planning and dosimetry accuracy. Our results showed that the residual distortion errors are less than 1 cm and will have a negligible clinical impact for more than 90% of the prostate patients whose lateral dimensions are < 40 cm (Chen et al 2004a)

3) We also studied structure volume differences between CT and MRI on the AcQSim and Corvus systems, which led to small discrepancies in DVH curves for those structures with significant differences. These differences reflected the inherent uncertainties of target and structure delineation using different imaging modalities and different treatment planning systems. However, these DVH discrepancies will not be a problem when MRI is used alone for treatment planning since both structure contouring and treatment optimization will be performed using the same imaging modality (Chen et al 2004a, 2004b).

4) We evaluated MRI- and CT-based IMRT treatment optimization for plan consistency. Since both planning techniques will be used clinically and in different treatment protocols it is essential to ensure IMRT plans using both imaging modalities are consistent in terms of target coverage, dose conformity and normal tissue sparing. Our results showed that no clinically significant differences were found between MRI- and CT-based treatment plans using the same beam arrangements, dose constraints and optimization parameters (Chen et al 2004b).

5) We validated the dosimetry accuracy of MRI-based treatment planning by recomputing MRI-based IMRT plans using patient CT data and an IMRT QA phantom. The differences in dose distributions between MRI plans and the corresponding recomputed plans were generally within 3%/3mm. The differences in isocenter doses between MRI dose calculation and phantom measurements were within our clinical criterion of 4% (Chen et al 2004a).

6) We also investigated the creation of MRI-based DRRs to facilitate initial patient setup. CT-based DRRs are routinely used for patient treatment setup verification by comparing with portal film or electronic portal imaging devices (EPID). However, directly MRI-derived DRRs do not provide enough bony structure information and therefore cannot be used directly for checking patient positions. To overcome this problem, a practical method to derive MRI-based DRRs for IMRT prostate patient setup has been developed. The relevant bony structures on MRI including pubic symphysis, femoral heads and acetabulum are contoured and assigned a bulk density of 2.0 g/cm^3. The bony structures are then clearly shown on the MRI-derived DRRs and can be used for patient treatment setup verification. The accuracy of this method has been verified by comparing with CT derived DRRs and the agreement between the two methods are estimated to be 2-3 mm based on 18 patients investigated (Chen et al 2004a).

<u>Validate and improve gradient distortion correction for MRI-based treatment planning</u>

The goal of our study is to provide "correct" pelvic images in which geometrical distortions are reduced to < 2 mm for target delineation and < 5 mm for external contour determination (which will be

used to define patient geometry for dose calculation). This will require an assessment of the sources and magnitudes of the different contributions to distortions in images acquired using our 0.23 T MRI unit. In order to achieve the goal, first we quantified the residual distortions for 15 patients. The residual error was within 1 cm for patients with lateral dimensions < 40 cm. The values determined this way should have included the residual MRI distortions (both system related and object induced), differences in external contours due to patient setup between CT and MRI simulation, and the errors introduced by image fusion, which was estimated to be at the 2-3 mm level, which was achieved routinely in our clinic. The object induced effects are a result of both chemical shift and susceptibility effects due to the differences in the resonant frequency between fat and water and the magnetic field distortions introduced at tissue-air interfaces. The chemical shift artifacts and susceptibility distortion are larger on high-field MR units than on lower-field MR units. While chemical shift artifacts and susceptibility distortion can cause significant spatial misregistrations at high fields, their impact on MRI at lower fields is substantially reduced. For fields below about 0.5 Tesla (T), imaging sequences that provide a sufficient signal to noise ratio keep geometric distortion due to either of these object-related effects below 1-2 pixels. This is achieved by defining a lower limit for the bandwidth of the readout gradient during image acquisition. One in vivo study has shown that with 0.2 T using a bandwidth readout gradient >100 Hz/pixel in frequency direction there is no artifact detected (Fransson et al 2001). In our clinical routine MR simulation we have chosen 154 Hz/pixel in the frequency encoding direction, therefore the effects caused by chemical and susceptibility are considered negligible. In this study we aimed on correction of the residual distortion after GDC correction due to system induced distortion. We performed phantom measurements to calibrate/quantify MRI distortion at different axial planes to derive distortion maps for phantom of different sizes. We have compared these maps with the measured distortion using real patients by comparisons with CT images. A point-by-point mapping technique was developed and a computer software for improving the residual distortion using this method was also generated. Our results showed that by using this technique the residual distortion can be reduced to < 3 mm for patient lateral sizes up to 42 cm. A manuscript entitled "Investigation of MRI distortion for MR-based treatment planning for radiotherapy of prostate cancer" is in preparation (Chen et al 2005).

Investigate the effect of intra-fraction prostate motion

Prostate motion affects the treatment outcome. The movement of the prostate (relative to the skin marks or bony structures) between treatments (inter-fraction motion) is mainly caused by the filling of the bladder and the rectum. The effect of inter-fraction prostate motion can be corrected effectively by locating the prostate prior to treatment. At FCCC, either the BAT system or CT on rails is used to localize the prostate prior to every IMRT treatment. This can ensure the localization accuracy to about 3-5 mm. Bladder and rectal filling may also affect the prostate position during a treatment (intra-fraction motion). We have performed measurements to evaluate the intra fraction motion of prostates. Patients underwent MRI scans in the treatment position before radiation treatment. Axial and saggital cine images were obtained at the prostate. The images were updated for every 2 seconds for 2 minutes. Prostate motion was scored as the greatest displacement of the prostate seen among the 60 images in the superior-inferior, anterior-posterior, and lateral planes. For this study, all the image data have been collected. The dada analysis is in progress.

Investigate the accuracy of a stereotactic body frame for patient immobilization

We performed MRI for different target localization and patient immobilization techniques to quantify the effect of prostate motion, and then to determine special treatment margins correspondingly. These

will include alpha-cradle alone, and a stereotactic body frame from Radionics (Boston, MA). A Radionics Body Frame localizing system has been investigated at FCCC for accurate immobilization of patients undergoing stereotactic radiosurgery/therapy (SRS/SRT) using a stereotactic IMRT optimization software and a micro multileaf collimator (mMLC) (Wang et al 2004a, 2004b). The body system is a whole body fixation system using airflow modules, a vacuum system and fixation sheets. The treatment area will be covered with a fixation sheet. When the vacuum system is turned on, the space around the patient between the vacuum cushion and the sheet is evacuated and the sheet is sucked against the vacuum cushion. The sheet nestles against the patient's body producing a uniform fixation to the body surface without causing impression.

To study the patient immobilization and target localization accuracy for this body system, we used the 0.23 T MRI to collect sequential axial and sagittal images of prostate patients. Each patient underwent one scan per week for 4 weeks. For this study, a fast image is required. The temporal resolution requires shorter than the breathing cycle (approximately 2.5 s) to measure respiration-related motion. We scanned the patients in both axial and sagittal planes respectively. T1 weighted FSE images with cines at 3 mm slice thickness with 60 images obtained every 2 seconds (TR/TE = 18/8 ms, FOV = 475 mm, Matrix = 128 x 256, ETL = 1, scan time 2 s) were obtained based on our pilot experiment. The prostate replacement will be measured on MRI console in three dimensions on both axial and sagittal images and the absolute values of the displacement calculated based on pixel value. This experimental procedure was repeated without the vacuum body frame. The replacement of the prostate was compared between with and without the body frame. This can help us quantify the improvement with the body frame. For this study, we are in the processing of the data analysis.

Key Research Accomplishments

We have accomplished the following tasks:

- We have verified the dosimetry accuracy of prostate treatment planning using homogeneous patient geometry by doing dose calculations on CT with and without heterogeneity correction for 15 patients.
- We have evaluated the dosimetric accuracy of CT- and MRI-based treatment planning using homogeneous geometry using AcQSim planning system.
- We have investigated the effect of MRI residual distortion after GDC on IMRT treatment planning and dosimetry accuracy.
- We have studied structure volume differences between CT and MRI on the AcQSim and Corvus system.
- We have evaluated MRI- and CT-based IMRT treatment optimization for plan consistency.
- We have validated the dosimetry accuracy of MRI-based treatment planning by recomputing MRI-based IMRT plans using patient CT data and an IMRT QA phantom.

Reportable Outcomes

Peer-reviewed papers resulting from or supported in part by this grant:

- Breen MS, Butts K, **Chen L**, Saidel GM, Wilson DL. MRI-Guided Laser Thermal Ablation Therapy: Model and Parameter Estimates to Predict Cell Death from MR Thermometry Images.*IEEE Transactions in Medical Imaging.* Submitted (2004)

- **Chen L,** Price RA Jr., Wang L, Li JS, Qin L, Ding M, Palacio E, T-B Nguyen, Ma C-M, Pollack A. Dosimetric evaluation of MRI-based treatment planning for prostate cancer. *Phys. Med. Biol.* 49: 5157-5170 (2004).

- **Chen L,** Price RA Jr., Wang L, Li JS, Qin L, Shawn M, Ma C-M, Freedman GM and Pollack A . MRI-Based Treatment Planning for Radiotherapy: Dosimetric Verification for Prostate IMRT. *International Journal of Radiation Oncology Biology Physics* 60(2): 636-47 (2004)

- **Chen L,** Li JS, Price RA et al. Investigation of MR-Based Treatment Planning for Lung and Head & Neck using Monte Carlo Simulations *The XIVth Internatinal Conference on the use of Computers in Radiation Therapy* 520-523, 2004

- Li JS, Freedman GM, Price R, Wang L, Anderson P, **Chen L**, Xiong W, Yang J, Pollack A and Ma C-M. Clinical implementation of intensity-modulated tangential beam irradiation for breast cancer. Med. Phys. 31 (5), 1023-1031 (2004)

- Ma CM, Price RA Jr. Li JS, **Chen L**, Wang L, Fourkal E, Qin L and Yung J . Monitor unit calculation for Monte Carlo treatment planning. *Phys. Med. Biol.49 1671-1687* (2004)

- Ma, C.M, Li, J.S, Pawlicki, T, Jiang, S.B, Deng, J, Price, R.A. **Chen, L,** Wang, L, Fourkal, E, Qin, L.H., Yang, J, Xiong, W. MCSIM - A Monte Carlo Dose Calculation Tool for Radiation Therapy. *Proc. of the XVIth International Conference on the Use of Computer in Radiation Therapy* (ICCR, Seoul, 2004) pp515-9.

- Qin, L, Li, J.S, Price, R.A, **Chen, L**, McNeeley, S, Ding, M, Fourkal, E, Freedman, G, Ma, C.M. A Monte Carlo Based Treatment Optimization Tool for Modulated Electron Radiation Therapy. *Proc. of the XIVth International Conference on the Use of Computer in Radiation Therapy* (ICCR, Seoul, 2004) pp527-30.

- Qin, L, **Chen, L,** Li, J.S, Price, R.A, Yang, J, Xiong, W, Ma, C.M. Phase Space Analysis of Siemens Electron Beams for Monte Carlo Treatment Planning. *Proc. of the XIVth International Conference on the Use of Computer in Radiation Therapy* (ICCR, Seoul, 2004) pp665-8.

- Wang L, R Jacob, **Chen L**, Feigenberg S, Konski A, Ma C and B Movsas. Stereotactic IMRT for prostate cancer: Setup accuracy of a new stereotactic body localization system. *Journal of Applied Clinical Medical Physics* 5: 18-28 (2004a)

- Wang L, Movsas B, Jacob R, Fourkal E, **Chen L**, Price R, Feigenberg S, Konski A, Pollack A and Ma C. Stereotactic IMRT for prostate cancer: Dosimetric impact of multileaf collimator leaf width in the treatment of prostate cancer with IMRT. *Journal of Applied Clinical Medical Physics* 5: 29-41 (2004b)

- Wang, L, Hoban, P, Paskalev, K, Yang, J, Li, J. S, **Chen, L,** Xiong, W, Ma, C.M. Dosimetric Advantage and Clinical Implication of a micro-Multileaf Collimator in the Treatment of Prostate with Intensity Modulated Radiotherapy. *Medical Dosimetry*. in press (2005).

- Xiong W, Li J, **Chen L**, Price RA, Freedman G, Ding M, Qin L, Yang J and Ma C-M. Optimization of combined electron and photon beams for breast cancer. *Phys. Med. Biol.* 49 1973-1989 (2004)

- Yuh EL, Shulman SG, Mehta SA, Xie J, **Chen L,** Frenkel V, Bednarski MD and Li KCP. Delivery of a Systemic Chemotherapeutic Agent to Tumors Using Focused Ultrasound – A study in a murine model *Radiology* In press (2005)

- Yang J, Li J, **Chen, L** Price RA, McNeeley S, Qin L, Wang, L, Xiong W and Ma C-M. Monte Carlo evaluation of heterogeneity effect in IMRT treatment planning for prostate cancer *Phys. Med. Biol.* In Press (2005)

Non peer-reviewed papers resulting from or supported in part by this grant:

- **Chen L.** Magnetic resonance has proven useful in radiation therapy simulation and treatment planning for prostate intensity-modulated radiation therapy *Advance for Imaging and Oncology* 14 57-58 (2004)

Meeting abstracts resulting from or supported in part by this grant:

- **Chen L**, Konski A, Chen Z, Price R, Li J, Wang L, Qin L, Ma C. MRI study of tumor motion for radiation treatment planning. Proc. Medical Physics, 31(6), 1904, 2004.

- **Chen L**, Chen Z, Price R, Li J, Wang L, Qin L, Ma C. Treatment setup for MRI-based treatment planning for prostate IMRT. Proc. Medical Physics, 31(6), 1925, 2004.

- Wang L, Feigenberg S, paskalev K, **Chen L,** Qin L, Ma C, Movsas B. Optimal treatment planning of extracranial stereotactic conformal radiotherapy for medically inoperable lung cancer. Proc. ASTRO 2004

- Wang L, Ma C, Paskalev K, Jacob R, **Chen L**, Feigenberg S, Movsas B. Feasibility study for clinical implementation of dose hypofractionation with IMRT for prostate cancer. Proc. Medical Physics, 31(6), 1788, 2004

- Qin L, Xiong W, Yang J, Li J, McNeeley S, **Chen L**, Price R, Ma C. Investigation of an electron specific multileaf collimator for modulated electron radiation therapy. Proc. Medical Physics, 31(6), 1798, 2004. Proc. Medical Physics, 31(6), 1798, 2004.

- Li J, Wang L, **Chen L**, Yang J, Ma C. Monte carlo dose verification for IMRT plan delivered using micromultileaf collimators. Proc. Medical Physics, 31(6), 1844, 2004.

- Qin L, Yang J, Li J, **Chen L**, Proce R, Ma C. Effect of voxel size on monte carlo dose calculations. Proc. Medical Physics, 31(6), 1883, 2004.

- Chen Z, Ma C, Paskalev K, Richardson T, Palacio L and **Chen L**. Image distortion corrections for MRI based treatment planning. Proc. Medical Physics, 31(6), 1890, 2004.

- Ma C, Xiong W, Yang J, Price R, **Chen L**, Pollack A. Image guided therapy: Aiming at clonogenic cells or hypoxic cells? Proc. Medical Physics, 31(6), 1890, 2004.

- Chen Z, Ma C, Palacio L, Richardson T, Paskalev K and **Chen L**. Investigation of CT-MRI image intensity correlation for MRI-based dose calculation. Proc. Medical Physics, 31(6), 1897, 2004.

Funding applied for based on work resulting from or supported in part by this grant:

NIH R01 (PI: Wang L): Improving treatment accuracy for hypofractionated SRT (submitted in Oct. 2004)

Conclusions

We have made significant progress during our first-year investigation. We have successfully performed the tasks scheduled in the "Statement of Work". We have confirmed that treatment planning dose calculations using MRI-derived homogenous geometry are adequate for patient sizes within 38 cm after MR image distortion is corrected using the GDC software. We have investigated the effect of MRI residual distortion after GDC on IMRT treatment planning and dosimetry accuracy. We evaluated MRI- and CT-based IMRT treatment optimization for plan consistency. We have validated the dosimetry accuracy of MRI-based treatment planning by recomputing MRI-based IMRT plans using patient CT data and an IMRT QA phantom.

Note on Human Subject Protection Approval

In the original proposal the research was considered to be under two existing approved IRBs (IRB# 03-815 and 02-604). However, based on the suggestions from the DOD human protection specialist, a separate IRB for this study would be more appropriate. Therefore, we obtained a separate IRB (IRB# 04-848) for this project and submitted the paper work to DOD in Nov. 2004, which is now under review and pending approval. The research work reported here was accomplished under the local approved IRB and supported by institutional funds.

References

Chen L, Price RA Jr., Wang L, Li JS, Qin L, Ding M, Palacio E, T-B Nguyen, Ma C-M, Pollack A. Dosimetric evaluation of MRI-based treatment planning for prostate cancer. *Phys. Med. Biol.* 49: 5157-5170 (2004a).

Chen L, Price RA Jr., Wang L, Li JS, Qin L, Shawn M, Ma C-M, Freedman GM and Pollack A . MRI-Based Treatment Planning for Radiotherapy: Dosimetric Verification for Prostate IMRT. *International Journal of Radiation Oncology Biology Physics* 60(2): 636-47 (2004b)

Fransson A, Andreo P, Potter R. Aspects of MR image distortions in radiotherapy treatment planning. *Strahlenther Onkol* 2002; 177:59-73.

Wang L, Movsas B, Jacob R, Fourkal E, Chen L, Price R, Feigenberg S, Konski A, Pollack A and Ma C. Stereotactic IMRT for prostate cancer: Dosimetric impact of multileaf collimator leaf width in the treatment of prostate cancer with IMRT. *Journal of Applied Clinical Medical Physics* 5: 29-41 (2004)

Wang L, R Jacob, Chen L, Feigenberg S, Konski A, Ma C and B Movsas. Stereotactic IMRT for prostate cancer: Setup accuracy of a new stereotactic body localization system. *Journal of Applied Clinical Medical Physics* 5: 18-28 (2004)

Chen Z, C-M Ma, Paskalev K, Li J, Richardson T, Palacio L and Chen L. "Investigaton and correction of MRI distortion for MR-based treatment planning for radiotherapy of prostate cancer" in preparation 2005

Appendices

List of published papers quoted in the body of text:

Chen L, Price RA Jr., Wang L, Li JS, Qin L, Ding M, Palacio E, T-B Nguyen, Ma C-M, Pollack A. Dosimetric evaluation of MRI-based treatment planning for prostate cancer. *Phys. Med. Biol.* 49: 5157-5170 (2004a).

Chen L, Price RA Jr., Wang L, Li JS, Qin L, Shawn M, Ma C-M, Freedman GM and Pollack A . MRI-Based Treatment Planning for Radiotherapy: Dosimetric Verification for Prostate IMRT. *International Journal of Radiation Oncology Biology Physics* 60(2): 636-47 (2004b)

INSTITUTE OF PHYSICS PUBLISHING PHYSICS IN MEDICINE AND BIOLOGY

Phys. Med. Biol. 49 (2004) 5157–5170 PII: S0031-9155(04)84011-9

Dosimetric evaluation of MRI-based treatment planning for prostate cancer*

L Chen, R A Price Jr, T-B Nguyen, L Wang, J S Li, L Qin, M Ding, E Palacio, C-M Ma and A Pollack

Radiation Oncology Department, Fox Chase Cancer Center, Philadelphia, PA 19111, USA

E-mail: Lili.Chen@fccc.edu

Received 23 July 2004, in final form 23 September 2004
Published 29 October 2004
Online at stacks.iop.org/PMB/49/5157
doi:10.1088/0031-9155/49/22/010

Abstract

The purpose of this study is to evaluate the dosimetric accuracy of MRI-based treatment planning for prostate cancer using a commercial radiotherapy treatment planning system. Three-dimensional conformal plans for 15 prostate patients were generated using the AcQPlan system. For each patient, dose distributions were calculated using patient CT data with and without heterogeneity correction, and using patient MRI data without heterogeneity correction. MR images were post-processed using the gradient distortion correction (GDC) software. The distortion corrected MR images were fused to the corresponding CT for each patient for target and structure delineation. The femoral heads were delineated based on CT. Other anatomic structures relevant to the treatment (i.e., prostate, seminal vesicles, lymph notes, rectum and bladder) were delineated based on MRI. The external contours were drawn separately on CT and MRI. The same internal contours were used in the dose calculation using CT- and MRI-based geometries by directly transferring them between MRI and CT as needed. Treatment plans were evaluated based on maximum dose, isodose distributions and dose–volume histograms. The results confirm previous investigations that there is no clinically significant dose difference between CT-based prostate plans with and without heterogeneity correction. The difference in the target dose between CT- and MRI-based plans using homogeneous geometry was within 2.5%. Our results suggest that MRI-based treatment planning is suitable for radiotherapy of prostate cancer.

(Some figures in this article are in colour only in the electronic version)

* The materials in this paper have been presented in part at the San Diego 2003 AAPM.

0031-9155/04/225157+14$30.00

1. Introduction

Radiation therapy is one of the most effective treatment modalities for prostate cancer. Many investigators have demonstrated that dose escalation with three-dimensional (3D) conformal radiation therapy (3DCRT) and recently intensity-modulated radiation therapy (IMRT) potentially increases the cure rate while keeping complication risk at a reasonable level (Zelefsky *et al* 1998, Hanks *et al* 1998, Hanks 1999, Pollack *et al* 1999, 2000, 2002, Yeoh *et al* 2003). As dose levels are increased, the precise knowledge of target location and size and the accuracy of dose delivery become crucial. Magnetic resonance imaging (MRI) provides superior image quality for soft-tissue delineation over computed tomography (CT) and is widely used for target and organ delineation in radiotherapy for treatment planning (Khoo *et al* 2000, Tanner *et al* 2000, Potter *et al* 1992). The prostate volume on CT appears to be about 40% larger than on MRI (Rasch *et al* 1999). These results were consistent with those reported by Krempien *et al* (2002). Debois *et al* (1999) showed that improved prostate and rectal volume delineation from MRI could lead to improvements both in target coverage and rectal sparing. As a result of improved soft-tissue delineation the utilization of MRI for treatment planning of prostate cancer is desirable. Studies have been carried out to explore the efficacy of the use of MRI for radiotherapy treatment planning (Beavis *et al* 1998, Mah *et al* 2002a, 2002b, Michiels *et al* 1994, Mizowaki *et al* 2000, Lee *et al* 2003).

However, several perceived disadvantages of using MRI for treatment planning dose calculation have precluded its widespread use in this area. These disadvantages include the lack of electron density information for accurate dose calculation and image distortion leading to geometrical inaccuracies. Currently, MR and CT image fusion with CT-based dose calculation is the gold standard for prostate treatment planning. Although MR-CT image fusion has been widely accepted as a practical approach for both accurate anatomical delineation (using MRI data) and dose calculation (using CT data) it would be ideal if MRI could be used alone for prostate treatment planning (i.e., MRI-based treatment planning). The fusion process introduces additional error since it is often difficult to coordinate the CT and MR images, and substantial differences in bladder and rectal filling may lead to significant discordance. Furthermore, MRI-based treatment planning will avoid redundant CT imaging sessions, which in turn will avoid unnecessary radiation exposure to the patient. It also saves patient, staff and machine time.

Regarding the lack of electron density information in MRI, many studies have shown that there is no clinically significant difference in dose calculation between homogeneous and heterogeneous geometry for the pelvic region (Ma *et al* 1999, 2000, Chen *et al* 2002, Yang *et al* 2004). It has been common practice to use homogeneous geometry in treatment planning dose calculation for prostate cancer both for conventional treatment and IMRT. Therefore, the lack of electron density information in MRI is not considered to be a significant problem in terms of treatment planning accuracy for prostate cancer. This assumption is carefully examined in this work to provide a basis for MRI-based dose calculation, in which all the internal organs and structures (including the target) are delineated on MRI and the dose calculation is performed on homogeneous geometry built from the patient external contour drawn on MRI.

It is clear that before MRI alone can be used for treatment planning any significant image distortions must be quantified and corrected. Image distortion arises from both system-related effects and object-induced effects. System-related distortion is a result of inhomogeneities in the main magnetic field and non-linearities in spatial encoding gradient field while object-induced effects are a result of both chemical shift and susceptibility effects due to the differences in the resonant frequency between fat and water and the magnetic field

distortions introduced at tissue–air interfaces. The chemical shift artefacts and susceptibility distortion are larger on high-field MR units than on lower field MR units. While chemical shift artefacts and susceptibility distortion can cause significant spatial misregistrations at high fields, their impact on MRI at lower fields is substantially reduced. For fields below about 0.5 Tesla (T), imaging sequences that provide a sufficient signal-to-noise ratio keep geometric distortion due to either of these object-related effects below 1–2 pixels. This is achieved by defining a lower limit for the bandwidth of the readout gradient during image acquisition. One *in vivo* study has shown that with 0.2 T using a bandwidth readout gradient >100 Hz/pixel in frequency direction there is no artefact detected (Fransson *et al* 2001). In our clinical routine MR simulation, we have chosen 154 Hz/pixel in the frequency encoding direction, therefore the effects caused by chemical and susceptibility are considered negligible. For system-related distortions, different image distortion correction methods have been developed (Finnigan *et al* 1997, Fransson *et al* 1998, Schad *et al* 1987, 1992, Schubert *et al* 1999). Mah *et al* (2002a) showed that with a gradient distortion correction (GDC) the distortions of the external contour from MRI were insignificant for 3DCRT of prostate cancer, based on the tissue-maximum ratio (TMR) analysis using a 0.23 T open system and a 1.5 T closed system.

The objective of the current investigation is to directly compare the dosimetric accuracy of CT- and MRI-based treatment planning for prostate cancer for 15 patients using a commercially available treatment planning system—the AcQPlan system. We verify the assumption of the use of homogeneous geometry for dose calculation for prostate by comparing 3DCRT plans using CT-based dose calculation with and without heterogeneity correction. We quantify the residual MRI distortions with the use of the GDC software and examine their effect on the determination of external contours and dose distributions. The use of MRI-based digitally reconstructed radiographs (DRRs) for patient set-up is also discussed.

2. Materials and methods

2.1. The MRI scanner

A 0.23 T open MRI scanner (Philips Medical Systems, Cleveland, OH) was used for this study. The MR scanner consists of two poles of approximately 1 m diameter each. The separation between the two poles is 47 cm. The MR scan table can be moved in orthogonal planes along a set of rails mounted on the floor and on an orthogonal set of rails built in the couch. A flat table top made of special material, which is stiff and light, was inserted beneath the patient. A set of pads made of special foam was used to adjust the table height according to the patient size. The three triangulation lasers (centre and laterals) identical to those used on linear accelerators were used for patient positioning.

2.2. CT imaging procedure

All the patients were required to have a full bladder and were scanned in a supine position in a customized alpha cradle with knee support and a foot holder. Patients were scanned on a CT simulator (PICKER PQ 5000, Philips Medical Systems, Cleveland, OH) with a field of view (FOV) of 480 mm, matrix 512 × 512 (resolution 0.94 mm) and slice thickness 3 mm. The axial CT slices extended from the third lumbar vertebrae to the middle of the femurs. Three steel ball fiducials (1 mm in diameter) were used (one anterior and two laterals) on the skin surface to mark the centre of the prostate as an isocentric slice. Then skin tattoos were aligned with the fiducial markers for daily treatment set-up. The CT data were transferred

Figure 1. An MR image showing a special fiducial marker for MR localization. The outer diameter of the marker is 1.5 cm. The inner diameter is 4 mm. The grey part with iodine provides the MR signal. The hollow centre shows clearly on a single slice.

to the treatment planning workstation and the patient was transferred to the MRI room for scanning within 0.5 h post CT.

2.3. MR imaging procedure

Patients were scanned in a supine position in an alpha cradle with knee support and a foot holder (the same position as for CT). Three donut shaped fiducials (figure 1) were superimposed on the tattoos that mark the centre of the prostate as indicated by CT. A series of 48 axial slices (3 mm thickness) covering the whole pelvis based on the guidance image were acquired using turbo pin echo, 3D sequence, TR/TE 3000/140 ms, FOV 45–50 cm (depending on patients' anatomical dimensions), matrix 256 × 256, echo train length (ETL) 32, flip angle 90°, slice thickness 3 mm, number of excitations (NEX) 1, bandwidth (BW) 39.5 kHz, frequency direction horizontal and 9 min scan time. The MR images were post-processed for image distortion correction using the GDC software provided by the vendor. The distortion corrected MR images were transferred to the treatment planning workstation.

2.4. Target and structure delineation

In our institution (FCCC), CT–MR fusion with CT-based dose calculation has been a routine procedure for all prostate cancer patients. Each patient underwent a CT and an MR scan as part of a routine simulation procedure. CT images were loaded as primary images and MR images were loaded as secondary images and then fused to the CT images using the software available in the AcQSim system. Fifteen patients were included in this study. The femoral heads were contoured based on CT and the targets and other critical structures were contoured based on MRI. The external contours were determined separately based on CT and MRI to define patient geometry for dose calculation. The same internal contours were used in both CT-based and MRI-based dose calculation. The differences in internal structure volumes between CT and MRI were studied, which were a result of contour transfer between image modalities due to the difference in the pixel size between CT and MRI. It was considered to be more reliable to use the same set of internal structure contours for the plan comparison than using a new set of contours generated on MRI since this would introduce additional uncertainties in the contours between MRI and CT. Although the CT and MRI scans were performed within a small time interval ($<1/2$ h) the difference in the rectal and bladder fillings could affect the volumes of these organs significantly.

2.5. Measurement of residual MR image distortion after GDC

In order to study the effect of residual MRI distortion on the dosimetric accuracy of MRI-based treatment planning, the patient dimensions in both anterior/posterior (AP) and lateral (LAT) directions were measured on MRI (after GDC) and compared with those measured on distortion-free CT images. The differences of the external contours between CT and MRI on the treatment isocentric slice were measured to estimate the error of residual MRI distortion. The values determined this way should have included the residual MRI distortions (both system related and object induced), differences in external contours due to patient set-up between CT and MRI simulation, and the errors introduced by image fusion, which was estimated to be at the 2–3 mm level, which was achieved routinely in our clinic. There were rejections occasionally, as determined by the treating physician, when significant differences were found in some internal structures due to large changes in the rectal and bladder fillings between CT and MRI but this was not the case for the 15 patients investigated in this work.

2.6. Dose calculations and evaluations

The AcQPlan system version 5 was used for the study, which is capable of performing dose calculation on both CT and MRI. A four-field 3D conformal planning technique was used for the study. First, we verified the dosimetry accuracy of using homogeneous geometry for prostate planning. This was done by calculating dose distributions using the distortion-free CT data with and without heterogeneity correction (equivalent TAR), respectively. As a result, two treatment plans were generated for each patient with the same treatment parameters (i.e., energy, gantry angle, block shape and size, and dose prescription). We used 10 or 18 MV photon beams with an 8 mm block margin around the planning target volume (PTV). Second, we evaluated the dosimetry accuracy of CT-based and MRI-based dose calculation. This was achieved by calculating dose distributions using both CT and MRI data without heterogeneity correction (i.e., using homogeneous geometry defined by the patient external contour). The same MUs obtained from CT-based plans were directly used in MRI-based plans so that the effects of residual MRI distortions on external contours and the differences in internal structure volumes between CT and MRI can be quantified. The plans were evaluated based on isodose distributions and dose–volume histograms (DVHs) for the target and the critical structures. Based on the DVHs, doses were reported at 95% of the planned treatment volume (PTV), D95, for the prostate, at 35% (D35) and 17% (D17) of the rectum volume, and at 50% (D50) and 25% (D25) of the bladder volume. These dose points were chosen based on our current clinical acceptance criteria for prostate cancer treatments.

3. Results and discussion

3.1. Measurement of residual MRI distortion and external contour

The GDC software improves MR image distortion significantly in the peripheral regions of the FOV, which is important to the accurate determination of patient external contours for MRI-based treatment planning. Figure 2 shows an example of the MR images before and after the gradient distortion correction. The effect of MR distortion on external contours was reduced significantly after the GDC. Similar improvement was observed for all patients investigated.

The residual distortions after the GDC along the major axes on the treatment isocentric slice were related to the patient anatomic size. Table 1 summarizes our results for 15 patients. As distortion increases with the distance between the magnetic isocentre and the point of

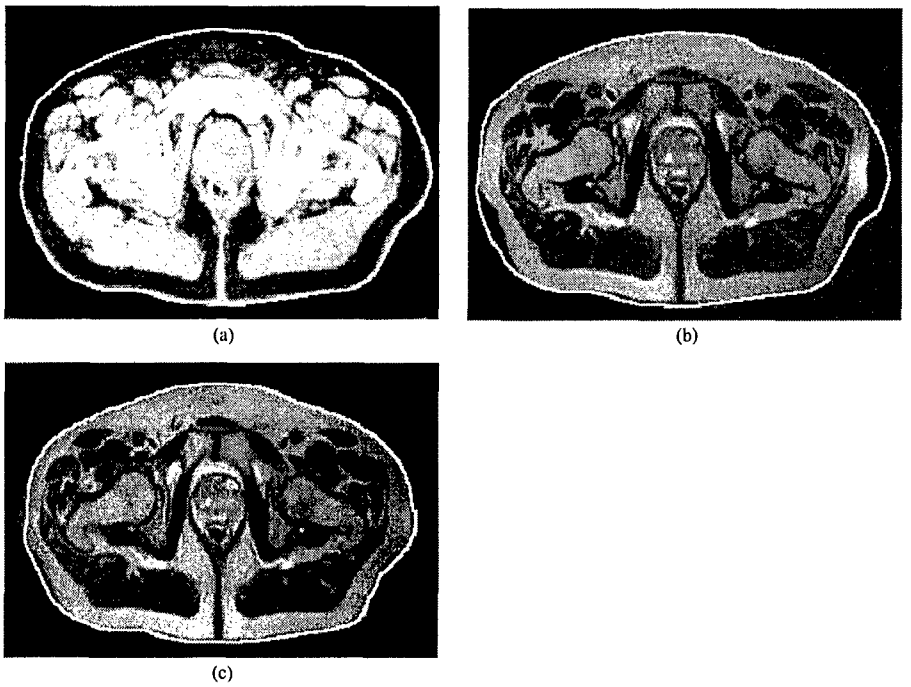

Figure 2. Comparison of CT and MR images for a prostate patient: (a) a distortion-free CT image, (b) an MR image before the GDC and (c) an MR image after the GDC.

interest, the distortion becomes significant when patient size is greater than a certain value. Our results showed that in the AP (anterior and posterior) dimension all measurements were less than 30 cm and there were no significant distortions in this direction. For the LAT (lateral) dimensions, the residual distortion was negligible (range 0–0.2 cm) for patient sizes less than 36 cm (see patients 10 and 14). For patient sizes between 36 and 38 cm (patients 2, 4, 9 and 11) the maximum distortion was 0.7 cm (range 0–0.7 cm). For patient sizes between 38.5–40 cm (patients 3, 12, 13 and 15) the maximum distortion was 1.0 cm (range 0.2–1.0 cm). For patient sizes larger than 40 cm (patients 1, 5, 6 and 8) the maximum distortion was 2.7 cm (range 0.3–2.7 cm). The exact reason for the large residual distortion at the peripheral regions was not found. There may be several possibilities. A major possibility was the difference between the theoretical magnetic field distribution calculated by the GDC software and the actual field distribution. Without knowing the actual gradient distortion accurately in the peripheral regions the GDC cannot make a perfect correction. A minor possibility was the combination of the large distortion and the limited FOV (45–50 cm). For patients greater than 40 cm (e.g., patients 1, 5 and 6 in table 1 are greater than 44 cm in lateral dimensions) part of the patient geometry may be outside the FOV due to MR distortion. This part of the geometry will not be recovered by the GDC software although physically it is within the FOV. It should be mentioned that the residual distortions shown in table 1 also included the changes in patient dimensions between CT and MRI simulation due to patient set-up and the error introduced by image fusion.

Our results are consistent with previous studies. Beavis *et al* (1998) reported maximum distortion errors of ± 1 mm for a 10 cm FOV and ± 2 mm for a 24 cm FOV. These results were

Table 1. Patient dimensions measured on CT (distortion free) and the residual distortions on MR calculated as the difference between external contour points along the major axes on the isocentric slice on CT and those on MRI.

	Dimension on CT (cm)		Residual distortion (cm)			
Patient no	A/P	R/L	Anterior	Posterior	Right	Left
1	28.0	45.4	0.0	0.0	2.7	1.7
2	21.0	38.0	0.0	0.0	0.0	0.6
3	22.5	38.8	0.0	0.0	0.8	0.7
4	21.5	36.7	0.0	0.0	0.0	0.0
5	26.0	44.1	0.0	0.0	1.1	1.6
6	25.9	44.5	0.4	0.4	2.2	0.7
7	21.8	37.0	0.0	0.0	0.7	0.0
8	26.6	43.0	0.0	0.3	1.4	0.3
9	22.0	36.4	0.0	0.2	0.5	0.0
10	19.1	34.3	0.0	0.0	0.0	0.0
11	20.6	37.0	0.0	0.2	0.5	0.3
12	21.8	39.3	0.0	0.0	0.8	0.2
13	25	39.9	0.0	0.0	1.0	0.5
14	21	34.6	0.0	0.0	0.0	0.2
15	24	38.5	0.0	0.0	0.7	0.8

similar to those reported by other investigators (Hill *et al* 1994, Mizowaki *et al* 2000). Our previous study (Mah *et al* 2002a) estimated that the effect of image distortion was clinically insignificant for the prostate targets and nearby critical structures; they were all within 15 cm of the isocentre and the distortion error was found to be less than 2 mm on our low-field MR unit. The effect of residual image distribution on dose calculation (e.g., the effect on DVH calculation) was considered to be negligible after the GDC. In fact, we expect that MRI-based treatment planning will result in more accurate DVH calculation because soft-tissue structures can be more accurately delineated on MRI due to its superior soft-tissue contrast and the elimination of errors in patient set-up between CT and MR scans and in image fusion. The distortion error is more pronounced for the external contours and its effect can be clinically significant since the external contours will define the homogenous patient geometry (and the beam paths). The uncertainty in the fiducial locations will also affect the determination of the isocentre. To ensure the accuracy of MRI-based treatment planning and its clinical implementation we have set a criterion for patient selection with maximum lateral dimensions less than 38 cm. For patient lateral sizes larger than 38 cm we still use the standard CT and MR fusion technique with CT-based dose calculation. Approximate 90% patients in our clinic have lateral dimensions less than 38 cm based on a separated study.

3.2. Measurement of internal structure volumes

Table 2 shows the volume differences between CT and MRI for the prostate targets, seminal vesicles (SV) and critical structures as measured on the AcQSim. These differences were introduced by the contour transfer process and were thought mainly due to the difference in image pixel size between CT (512 × 512 matrix) and MRI (256 × 256 matrix). Similar small differences were also observed when patient plans were transferred from the AcQSim to other treatment planning systems. For structures with a relatively small volume, such differences may have noticeable effects on the DVH comparison between MRI- and CT-based dose calculation (see section 3.4). However, this will no longer be a problem when both contouring and treatment planning are performed on MRI directly.

Table 2. Internal structure volumes measured on MRI and CT as reported by the AcQPlan system. The internal contours were directly transferred between MRI and CT.

	GTV (cm^3)		SV (cm^3)		Rectum (cm^3)		Bladder (cm^3)	
Patient no	MR	CT	MR	CT	MR	CT	MR	CT
1	36.8	34.6	6.1	5.8	101.5	95.0	97.5	92.6
2	36.7	34.4	N/A	N/A	84.4	78.5	129.1	123.9
3	65.0	62.3	N/A	N/A	52.3	48.2	128.7	124.9
4	60.1	57.1	12.7	12.0	75.3	70.7	81.0	77.8
5	97.8	94.4	16.9	16.3	125.9	120.4	68.5	65.4
6	140.0	134.4	6.2	6.0	101.5	95.2	121.0	115.8
7	70.9	67.4	5.9	5.5	58.2	53.0	175.1	168.1
8	67.3	64.6	9.1	8.6	47.4	46.1	201.4	194.9
9	58.7	56.0	5.0	4.9	60.4	56.0	284.0	274.8
10	48.5	46.3	11.0	10.5	54.9	51.6	216.4	210.8
11	33.1	31.2	6.2	6.0	41.3	38.2	60.7	58.1
12	31.9	30.4	3.1	3.1	67.3	63.8	168.5	165.0
13	38.1	36.8	5.0	4.9	59.2	54.9	172.7	168.4
14	63.5	61.8	12.6	12.0	55.3	51.4	91.9	90.1
15	70.2	67.6	9.9	9.4	55.4	51.2	106.6	103.7

Table 3. The per cent dose difference between CT plans calculated with and without heterogeneity correction (expressed as dose without correction minus dose with correction divided by the prescription dose).

Patient no	Max dose	D95 prostate	D17 rectum	D35 rectum	D25 bladder	D50 bladder
1	0.75	0.50	0.95	0.70	0.75	0.45
2	0.80	0.00	0.75	1.15	0.25	0.00
3	0.95	0.75	0.75	0.70	0.70	0.25
4	0.55	0.50	0.45	0.70	0.95	0.75
5	2.50	0.45	0.95	1.20	1.40	1.70
6	0.70	0.45	0.75	1.20	0.70	0.95
7	0.65	0.25	0.50	0.70	0.70	0.70
8	2.35	1.40	1.45	1.40	1.20	0.25
9	0.30	0.25	1.20	1.20	0.70	0.45
10	1.25	0.95	0.70	1.40	0.70	0.25
11	1.70	0.25	1.00	1.00	1.00	0.75
12	2.60	0.40	1.50	1.40	0.65	0.05
13	0.50	0.00	0.70	0.95	0.95	0.00
14	0.75	0.70	0.95	0.95	1.20	0.95
15	2.45	1.20	2.40	1.70	2.60	2.65
Mean ± SD	1.25 ± 0.83	0.54 ± 0.40	1.00 ± 0.49	1.09 ± 0.31	0.96 ± 0.53	0.66 ± 0.71

3.3. Dosimetric verification of prostate planning using homogeneous geometry

To verify the dosimetry accuracy of prostate treatment planning using homogeneous patient geometry, we have performed dose calculations on CT with and without heterogeneity correction. The difference in the isocentre dose (prescription point) using the same MUs for the two plans was within 2.6% for all the cases. This is equivalent to a 2.6% difference in the MUs used for the treatment if the same dose is prescribed at the isocentre. We also examined the volumetric dose differences between these plans. Table 3 summarizes the results of CT-based plans with and without heterogeneity correction for maximum dose, D95 for the

prostate target, D17 and D35 for the rectum, and D25 and D50 for the bladder. It shows clearly that the differences in maximum doses and all other dose parameters are clinically insignificant (<2.6% of the prescription dose). The mean values averaged over 15 patients for maximum doses, D95 for the prostate, D17 and D35 for the rectum, and D25 and D50 for the bladder are 1.25 ± 0.83%, 0.54 ± 0.4%, 1.0 ± 0.49%, 1.09 ± 0.31%, 0.96 ± 0.53% and 0.66 ± 0.71% of the prescribed target dose, respectively. Our results confirmed previous observations that the dose with heterogeneity correction is slightly lower than that without it because of the additional attenuation from the bones but it has no clinical significance for 3DCRT and IMRT dose calculation for the pelvic region (Ma *et al* 1999, 2000, Chen *et al* 2002, Yang *et al* 2004). However, the above results are useful in establishing a foundation for the dose comparison between CT- and MRI-based treatment planning using homogeneous geometry (see next section).

It has been common practice to use homogeneous geometry for prostate treatment planning. This is not only supported by the sufficient dosimetry accuracy as discussed above but also by other practical considerations in using homogeneous geometry for dose calculation in the pelvic region. One consideration is the use of contrast agents for imaging that sometimes changes the CT numbers in the bladder significantly. Unless one modifies these CT numbers manually, a significant change in the electron density of the bladder will occur and the target and other organ doses will be affected significantly if one applies heterogeneity correction. Another consideration is the occasional occurrence of large gas pockets in the rectum on the planning CT, which may affect the dose distribution and/or MU calculation significantly when heterogeneity correction is used. These gas pockets often show up briefly during imaging and treatment for some patients but have little effect on the treatment in reality. The use of homogeneous geometry will avoid this problem and provide more accurate dose calculation for the treatment. Furthermore, the use of homogeneous geometry for dosimetric evaluation of CT- and MRI-based dose calculation also eliminates the possibility of any dose differences caused by the particular dose calculation algorithm used.

3.4. Dosimetric evaluation of CT- and MR-based treatment plans

Based on the results described above, it is reasonable to evaluate the dosimetric accuracy of CT- and MRI-based treatment planning using homogeneous geometry following our clinical practice. Figure 3 shows the isodose distributions and DVHs for an MRI-based plan and a CT-based plan. It can be seen that the differences in both isodose distributions and DVHs between the two plans are not clinically significant. Similar agreement was found between the plans for the rest of the patients investigated. The difference in the isocentre dose (prescription point) for the two plans was within 2% for all cases. The volumetric dose difference between MRI-based planning and CT-based planning is summarized in table 4.

For all 15 patients investigated, the maximum difference is less than 1.5% in the maximum dose and less than 1% in D95 of the prostate between MR- and CT-based plans, indicating consistent dose calculation accuracy of CT- and MRI-based treatment planning. In general, the differences in the rectal D17 and D35 and the bladder D25 and D50 are within 4% of the prescription dose except for patient 1 and 12, who showed a −9.8% difference in rectal D35 and a −12.4% difference in bladder D25, respectively. Those discrepancies do not correlate with residual MRI distortions. As shown in table 1, large residual distortions (>1 cm) appeared for patients 1, 5, 6, 8 and 13 while larger dose discrepancies were found for patients 1 and 12. The residual MRI distortions should not affect the dose calculation significantly because most differences in the external contours along the beam incident directions were less than 1 cm. When multiple beams are used in a 3DCRT treatment, it is unlikely that a treatment plan will

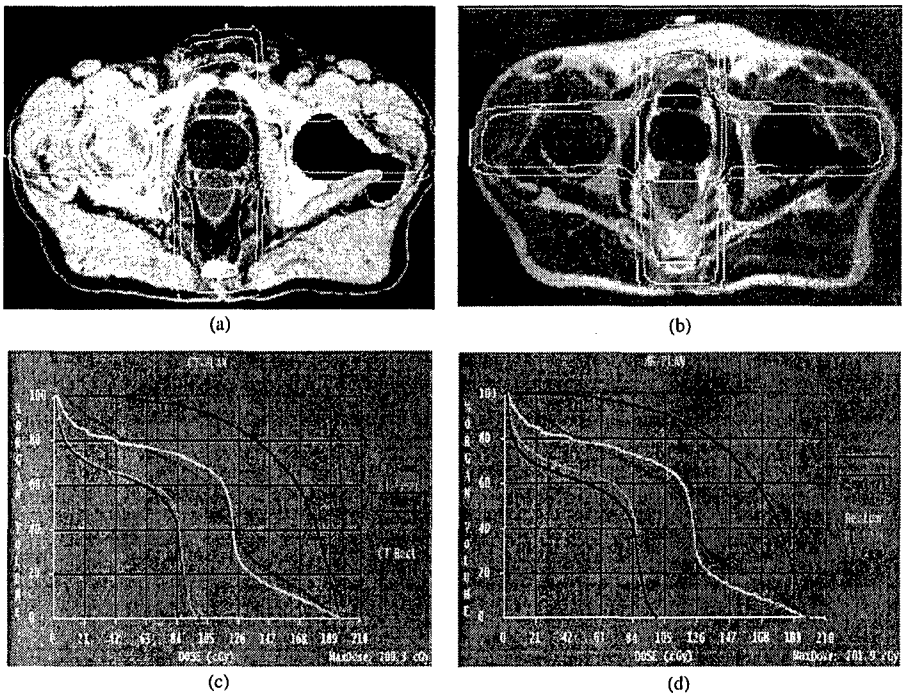

Figure 3. Comparison of isodose distributions based on CT (a) and MRI (b) and their corresponding DVHs for the PTV and critical structures based on CT (c) and MRI (d). The isodose lines represent 95%, 70%, 60%, 40% and 20% of the prescribed target dose.

Table 4. The per cent dose difference between MRI-based and CT-based plans calculated using homogeneous patient geometry (expressed as dose calculated on CT minus dose calculated on MRI divided by the prescription dose). The same monitor units derived from the CT plans were used for the dose calculation for the MRI-based plans.

Patient no	Max dose	D95 prostate	D17 rectum	D35 rectum	D25 bladder	D50 bladder
1	−0.60	−0.75	−0.25	−9.80	0.45	1.70
2	−1.50	−0.25	0.25	−0.70	−5.5	3.80
3	−0.05	0.00	−0.50	−0.50	0.00	0.50
4	−0.90	0.00	1.45	−0.25	−1.90	−0.50
5	−0.25	0.00	0.00	0.70	0.25	0.45
6	−0.45	−0.20	−0.50	−0.25	−0.45	0.00
7	−0.35	0.25	−1.45	−0.45	−0.20	0.00
8	−0.45	0.50	−0.70	−0.20	0.95	0.25
9	0.65	0.50	−0.50	0.00	−1.65	−3.30
10	0.10	0.25	0.70	−0.0	1.45	0.70
11	−0.25	0.25	−3.25	−1.00	0.75	0.25
12	0.50	0.25	0.00	0.00	−12.4	−1.90
13	−0.60	0.00	−1.20	0.00	1.90	0.75
14	−0.80	−0.25	2.15	0.75	−0.95	0.20
15	−0.25	0.00	−2.40	−0.20	1.20	1.15
Mean ± SD	−0.35 ± 0.54	0.04 ± 0.32	−0.41 ± 1.36	−0.81 ± 2.53	−1.07 ± 3.62	0.27 ± 1.56

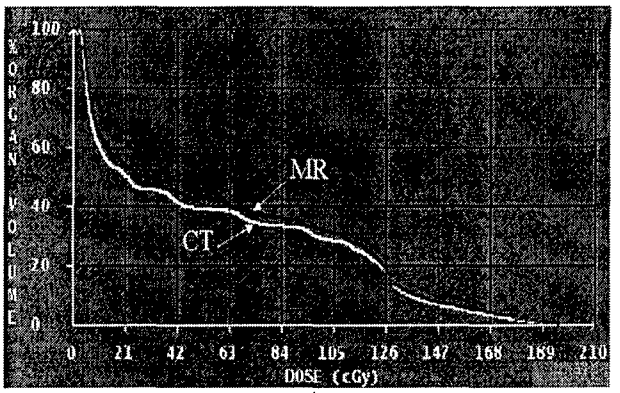

Figure 4. Comparison of DVHs for the rectum based on CT and MRI for patient 1. Since the DVH curves are 'flat' a small change in the rectal volume leads to a large change in the dose such as D35 but not in D17.

be affected significantly if only one or two beams are inaccurate by 1 cm in equivalent path length.

The large discrepancies for patient 1 and 12 are likely attributed to the differences in structure volumes between CT and MRI, which was mainly caused by the difference in pixel size between CT and MRI since we used the same internal contours and the contours were transferred directly from CT to MRI. These discrepancies also reflect the intrinsic uncertainty in contour determination using CT and/or MRI, which will not be a problem when only one image modality is used. A closer examination of the treatment plans for patients 1 and 12 reveals that the rectal and bladder DVH curves are very 'flat' at D35 and D25 for these two patients. The −9.8% difference in the rectal D35 corresponds to a 2.3% change in the rectal volume for patient 1 (see figure 4) and the −12.4% difference in the bladder D25 corresponds to a 4.7% change in the bladder volume for patient 12 (not shown). These are not unexpected because of the similar differences in the absolute volumes between CT and MRI for the two patients (see table 2).

A recent study by Lee *et al* (2003) also showed small differences in target and critical structure doses for five prostate cases planned separately using CT and MRI. The maximum difference was less than 3.2% in the maximum, minimum and mean target doses although the target volumes drawn on CT and MRI differed by more than 30% in some cases. This again indicated that accurate target delineation based on MRI will have a significant clinical impact for prostate treatment while dose calculation using homogeneous geometry based on MRI data is reasonable. They also investigated assigning a bulk density to the bones in MRI-based dose calculation and found the maximum dose difference was reduced marginally (from 3.2% to 2%). The maximum difference was 6.6% in the maximum rectal dose and 4.2% in the maximum bladder dose, respectively. The mean dose to the bladder and rectum was no longer meaningful due to the large differences in the rectum and bladder volumes (up to 500%) since there was no protocol to control the volumes between CT and MRI scans (possibly due to the large time intervals between the two scans).

3.5. MRI-based DRRs

CT-based DRRs are routinely used for patient treatment set-up verification by comparing with portal film or electronic portal imaging devices (EPID). However, MRI-derived DRRs do not

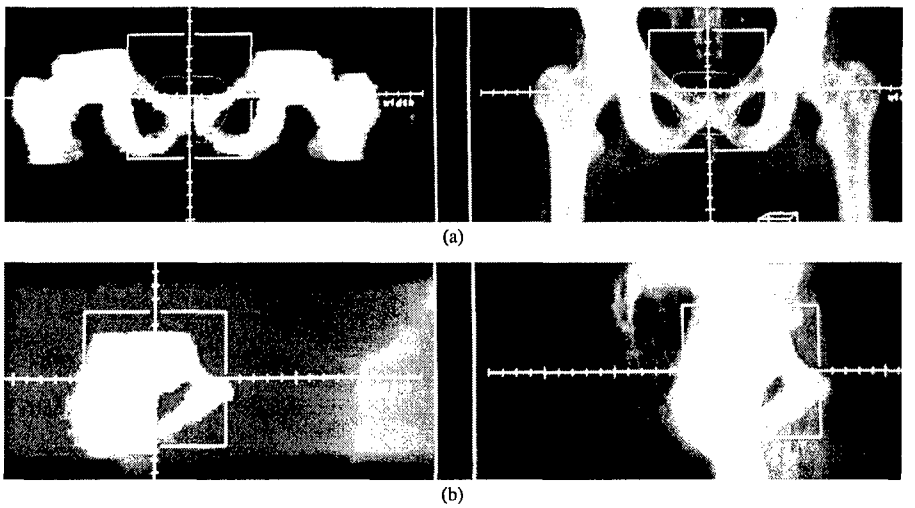

Figure 5. Comparison of MRI-based DRRs (left) and CT-based DRRs (right) for a prostate patient: (a) coronal view and (b) sagittal view.

provide enough bony structure information and therefore cannot be used directly for checking patient positions. To overcome this problem, a practical method to derive MRI-based DRRs for IMRT prostate patient set-up has been developed. The relevant bony structures on MRI including pubic symphysis, femoral heads and acetabulum are contoured and assigned a bulk density of 2.0 g cm^{-3}. The bony structures are then clearly shown on the MRI-derived DRRs and can be used for patient treatment set-up verification (figure 5). The accuracy of this method has been verified by comparing with CT-derived DRRs and the agreement between the two methods is estimated to be 2–3 mm based on 18 patients. At FCCC, we use an ultrasound target localization system (BAT, NOMOS, Sewickley, PA) for routine prostate treatment to improve patient set-up and target re-localization accuracy. MRI-derived internal contours actually provide better agreement with ultrasound images than CT-based contours and therefore result in better correction for prostate inter-faction motion. In our clinical implementation, MRI-based DRRs are used during initial treatment set-up together with BAT and later as a backup for the BAT system if a patient cannot be set up using BAT due to various reasons or if the BAT system is down.

4. Summary

The purpose of this study is to explore the use of MRI-based treatment planning for prostate cancer and to verify the dosimetry accuracy of its clinical implementation using a commercial treatment planning system. Our results confirm that treatment planning dose calculations using MRI-derived homogenous geometry are adequate for patient sizes within 38 cm after MR image distortion is corrected using the GDC software. MRI-derived DRRs utilizing the outlines of relevant bony structures are adequate for initial patient set-up. Further investigation of MRI-based treatment planning is being carried out for intensity-modulated radiation therapy of prostate cancer and other treatment sites.

Acknowledgments

This project was supported in part by grants from the DOD (PC030800) and the NIH (CA78331). We would also like to thank the support from Philips Medical Systems (Cleveland, OH), especially Dr Michael Steckner and David Abraham for their excellent technical assistance. We are indebted to Dr Gerald E Hanks for his foresight in initiating MRI-simulation at Fox Chase Cancer Center.

References

Beavis A W, Gibbs P, Dealey R A and Whitton V J 1998 Radiotherapy treatment planning of brain tumours using MRI alone *Br. J. Radiol.* **71** 544–8

Chen L, Li J, Mah D, Ma C-M, Wang L, Ding M, Freedman G, Movsas B and Pollack A 2002 Monte Carlo investigation of dosimetry accuracy for MR-based treatment planning *Med. Phys.* **29** 1339 (abstract)

Debois M *et al* 1999 The contribution of magnetic resonance imaging to the three-dimensional treatment planning of localized prostate cancer *Int. J. Radiat. Oncol. Biol. Phys.* **45** 857–65

Finnigan D J *et al* 1997 Distortion-corrected MR images for pelvic radiotherapy treatment planning *Proc. 19th L H Gray Conf.* chapter 3, pp 72–6

Fransson A, Andreo P and Potter R 2001 Aspects of MR image distortions in radiotherapy treatment planning. *Strahlenther. Onkol.* **177** 59–73

Fransson A *et al* 1998 System-specific geometric distortions in MR images from a 0.2 T resistive MRI unit *Radiother. Oncol.* **48** S187

Hanks G E 1999 Progress in 3D conformal radiation treatment of prostate cancer *Acta Oncol.* **38** 69–74

Hanks G E *et al* 1998 Dose escalation with 3D conformal treatment: five year outcomes, treatment optimization and future directions *Int. J. Radiat. Oncol. Biol. Phys.* **41** 501–10

Hill D L *et al* 1994 Accurate frameless registration of MR and CT images of the head: applications in planning surgery and radiation therapy *Radiology* **19** 447–54

Khoo V S, Adams E J, Saran F, Bedford J L, Perks J R, Warrington A P and Brada M 2000 A comparison of clinical target volumes determined by CT and MRI for the radiotherapy planning of base of skull meningiomas *Int. J. Radiat. Oncol. Biol. Phys.* **46** 1309–17

Krempien R C, Schubert K, Zierhut D, Steckner M C, Treiber M, Harms W, Mende U, Latz D, Wannenmacher M and Wenz F 2002 Open low-field magnetic resonance imaging in radiation therapy treatment planning *Int. J. Radiat. Oncol. Biol. Phys.* **53** 1350–60

Lee Y K, Bollet M, Charles-Edwards G, Flower M A, Leach M O, McNair H, Moore E, Rowbottom C and Webb S 2003 Radiotherapy treatment planning of prostate cancer using magnetic resonance imaging alone *Radiother. Oncol.* **66** 203–16

Ma C-M, Mok E, Kapur A, Findley F, Brain S, Forster F and Boyer A L 1999 Clinical implementation of a Monte Carlo treatment planning system *Med. Phys.* **26** 2133–43

Ma C-M, Pawlicki T, Jiang S B, Mok E, Kapur A, Xing L, Ma L and Boyer A L 2000 Monte Carlo verification of IMRT dose distributions from a commercial treatment planning optimization system. *Phys. Med. Biol.* **45** 2483–95

Mah D *et al* 2002a MRI Simulation: effect of gradient distortions on three-dimensional prostae cancer plans *Int. J. Radiat. Oncol. Biol. Phys.* **53** 757–65

Mah D, Steckner M, Palacio E, Mitra R, Richardson T and Hanks G E 2002b Characteristics and quality assurance of a dedicated open 0.23 T MRI for radiation therapy simulation *Med. Phys.* **29** 2541–7

Michiels J *et al* 1994 On the problem of geometric distortion in magnetic resonance images for stereotactic neurosurgery *Magn. Reson. Imaging* **12** 749–65

Mizowaki T, Nagata Y, Okajima K, Kokubo M, Negoro Y, Araki N and Hiraoka M 2000 Reproducibility of geometric distortion in magnetic resonance imaging based on phantom studies *Radiother. Oncol.* **57** 237–42

Pollack A, Zagars G K and Rosen I I 1999 Prostate cancer treatment with radiotherapy: maturing methods that minimize morbidity *Semin. Oncol.* **26** 150–61

Pollack A, Zagars G K, Smith L G, Lee J J, von Eschenbach A C, Antolak J A, Starkschall G and Rosen I 2000 Preliminary results of a randomized radiotherapy dose-escalation study comparing 70 Gy with 78 Gy for prostate cancer *J. Clin. Oncol.* **18** 3304–911

Pollack A, Zagars G K, Starkschall G, Antolak J A, Lee J J, Huang E, von Eschenbach A C, Kuban D A and Rosen I 2002 Prostate cancer radiation dose response: results of the M. D. Anderson phase III randomized trial *Int. J. Radiat. Oncol. Biol. Phys.* **53** 1097–105

Potter R, Heil B, Schneider L, Lenzen H, Al-Dandashi C and Schnepper E 1992 Sagittal and coronal planes from MRI for treatment planning in tumors of brain, head and neck: MRI assisted simulation *Radiother. Oncol.* **23** 127–30

Rasch C, Barillot I, Remeijer P, Touw A, van Herk M and Lebesque J V 1999 Definition of the prostate in CT and MRI: a multi-observer study *Int. J. Radiat. Oncol. Biol. Phys.* **43** 57–66

Schad L R *et al* 1992 Radiotherapy treatment planning of basal meningiomas: improved tumor localization by correlation of CT and MR imaging data *Radiother. Oncol.* **25** 56–62

Schad L *et al* 1987 Correction of spatial distortion in MR imaging: a prerequisite for accurate stereotaxy *J. Comput. Assist. Tomogr.* **11** 499–505

Schubert K *et al* 1999 Integration of an open magnetic resonance scanner in therapy simulation and three-dimensional radiation treatment planning *Strahlenther. Onkol.* **175** 225–31

Tanner S F, Finnigan D J, Khoo V S, Mayles P, Dearnaley D P and Leach M O 2000 Radiotherapy planning of the pelvis using distortion corrected MR images: the removal of system distortions *Phys. Med. Biol.* **45** 2117–32

Yang J, Li J, Chen L, Price R A, McNeeley S, Qin L, Wang L, Xiong W and Ma C-M 2004 Monte Carlo evaluation of heterogeneity effect in IMRT treatment planning for prostate cancer *Phys. Med. Biol.* at press

Yeoh E E K *et al* 2003 Evidence for efficacy without increased toxicity of hypofractionated radiotherapy for prostate carcinoma: early results of a Phase III randomized trial *Int. J. Radiat. Oncol. Biol. Phys.* **55** 943–55

Zelefsky M J *et al* 1998 Dose escalation with three-dimensional conformal radiation therapy affects the outcome in prostate cancer *Int. J. Radiat. Oncol. Biol. Phys.* **41** 491–500

Int. J. Radiation Oncology Biol. Phys., Vol. 60, No. 2, pp. 636–647, 2004

0360-3016/04/$–see front matter

ELSEVIER

doi:10.1016/j.ijrobp.2004.05.068

PHYSICS CONTRIBUTION

MRI-BASED TREATMENT PLANNING FOR RADIOTHERAPY: DOSIMETRIC VERIFICATION FOR PROSTATE IMRT

LILI CHEN, PH.D., ROBERT A. PRICE, JR., PH.D., LU WANG, PH.D., JINSHENG LI, PH.D., LIHONG QIN, PH.D., SHAWN MCNEELEY, M.S., C-M CHARLIE MA, PH.D., GARY M. FREEDMAN, M.D., AND ALAN POLLACK, PH.D., M.D.

Department of Radiation Oncology, Fox Chase Cancer Center, Philadelphia, PA

Purpose: Magnetic resonance (MR) and computed tomography (CT) image fusion with CT-based dose calculation is the gold standard for prostate treatment planning. MR and CT fusion with CT-based dose calculation has become a routine procedure for intensity-modulated radiation therapy (IMRT) treatment planning at Fox Chase Cancer Center. The use of MRI alone for treatment planning (or MRI simulation) will remove any errors associated with image fusion. Furthermore, it will reduce treatment cost by avoiding redundant CT scans and save patient, staff, and machine time. The purpose of this study is to investigate the dosimetric accuracy of MRI-based treatment planning for prostate IMRT.

Methods and Materials: A total of 30 IMRT plans for 15 patients were generated using both MRI and CT data. The MRI distortion was corrected using gradient distortion correction (GDC) software provided by the vendor (Philips Medical System, Cleveland, OH). The same internal contours were used for the paired plans. The external contours were drawn separately between CT-based and MR imaging–based plans to evaluate the effect of any residual distortions on dosimetric accuracy. The same energy, beam angles, dose constrains, and optimization parameters were used for dose calculations for each paired plans using a treatment optimization system. The resulting plans were compared in terms of isodose distributions and dose–volume histograms (DVHs). Hybrid phantom plans were generated for both the CT-based plans and the MR-based plans using the same leaf sequences and associated monitor units (MU). The physical phantom was then irradiated using the same leaf sequences to verify the dosimetry accuracy of the treatment plans.

Results: Our results show that dose distributions between CT-based and MRI-based plans were equally acceptable based on our clinical criteria. The absolute dose agreement for the planning target volume was within 2% between CT-based and MR-based plans and 3% between measured dose and dose predicted by the planning system in the physical phantom.

Conclusions: Magnetic resonnace imaging is a useful tool for radiotherapy simulation. Compared with CT-based treatment planning, MR imaging–based treatment planning meets the accuracy for dose calculation and provides consistent treatment plans for prostate IMRT. Because MR imaging–based digitally reconstructed radiographs do not provide adequate bony structure information, a technique is suggested for producing a wire-frame image that is intended to replace the traditional digitally reconstructed radiographs that are made from CT information. © 2004 Elsevier Inc.

Radiotherapy, MRI treatment planning, Prostate cancer, Dosimetry, IMRT.

INTRODUCTION

Prostate carcinoma is the most common malignancy in North American males and the second leading cause of cancer death. Disease confined to the prostate glad can be definitively treated with radical radiation therapy. However, in patients not achieving complete viable tumor clearance, a continued toll of local failure is observed (1). Recent investigations suggest that dose escalation with intensity-modulated radiation therapy (IMRT) potentially increases the local control while greatly reducing rectal and bladder exposure to high radiation doses (2–8). As dose levels are increased, the use of new imaging methods to more accurately target the prostate and the accuracy of dose delivery

Reprint requests to: Lili Chen, Ph.D., Radiation Oncology Department, Fox Chase Cancer Center, 333 Cottman Avenue, Philadelphia, PA 19111; Tel: (215) 728-3003; Fax: (215) 728-4789; E-mail: l_Chen@fccc.edu

The materials in this article have been partially presented at the ASTRO 2003 Annual Meeting in Salt Lake City.

Partially supported by grants from the NIH (CA78331) and DOD (PC030800).

Acknowledgments—We would like to thank Elizabeth A. Palacio and Teresa Richardson for help with MR scanning and Geraldine M. Shammo and Kevin L. Crawford for help with contouring and treatment planning. We would also like to thank the support from Philips Medical Systems, especially Dr. Michael Steckner and David Abraham for their excellent technical assistance.

Received Feb 24, 2004, and received in revised form May 26, 2004. Accepted for publication May 28, 2004.

become crucial. Magnetic resonance imaging (MRI) provides superior image quality for soft-tissue delineation over computed tomography (CT) and is widely used for target and organ delineation in radiotherapy for treatment planning (9–11). The prostate volume on CT appears much larger than on MRI (12). These results were consistent with those reported by Krempien *et al.* (13). Debois *et al.* (14) showed that improved prostate and rectal volume delineation from MRI could lead to improvements in both target coverage and rectal sparing. As a result of its improved soft-tissue delineation, using MRI for radiotherapy planning of prostate cancer is desirable. Although MRI-CT image fusion has been widely accepted as a practical approach for both accurate anatomic delineation (using MRI data) and dose calculation (using CT data), it would be ideal if MRI could be used alone for prostate treatment planning. The fusion process introduces additional error because it is often difficult to coordinate CT and magnetic resonance images, and differences in bladder and rectal filling may lead to substantial discordance. Furthermore, MRI-based treatment planning will avoid redundant CT imaging sessions, leading to reduced treatment cost and less radiation exposure to the patient.

More recently, studies have been carried out to explore the efficacy of MRI-based treatment planning for radiotherapy (15–22). However, the perceived disadvantages of using MRI for radiotherapy planning have precluded its widespread use in this area. These disadvantages include the lack of electron density information and image distortion leading to geometrical inaccuracies. MRI and CT image fusion with CT-based dose calculation is the gold standard for prostate treatment planning.

It has been generally accepted that there is no clinically significant difference in dose calculation between homogeneous and heterogeneous geometry assumptions for pelvic treatments. It has been common practice to use homogeneous geometry in treatment planning dose calculations for prostate cancer. This was also confirmed by Monte Carlo calculations for both conventional treatment and IMRT (23–25). Therefore, the lack of electron density information from MRI is not considered to be a significant problem in the context of treatment planning for prostate cancers.

Magnetic resonance imaging distortions affect the accuracy of dose calculation. It is clear that before MRI alone can be used for treatment planning for prostate patients, any image distortion must be quantified and corrected. Image distortion arises from both system-related effects and object-induced effects. System-related distortion is a result of inhomogeneities in the main magnetic and gradient fields, whereas object-induced effects are the result of both chemical shift and susceptibility effects because of the difference of the resonance between fat and water and the difference at tissue-air interfaces. For fields below about 0.5 T, imaging sequences that provide a sufficient signal-to-noise ratio maintain geometric distortion resulting from either of these object-related effects below 1–2 pixels. This is achieved by defining a lower limit for the bandwidth of the readout gradient during image acquisition (26). In our clinical MRI simulation routine, we have chosen 154 Hz/pixel in the frequency encoding direction; therefore, the effects caused by chemical and susceptibility are considered negligible. For system-related distortions, we have used gradient distortion correction (GDC) software to correct the MRI distortion. The GDC software was provided by the vendor (Philips Medical Systems, Cleveland, OH) and approved by the U.S. Food and Drug Administration. In this study, we explored the use of MRI-based treatment planning for prostate IMRT using the Corvus inverse planning system (NOMOS Corp., Sewickley, PA).

METHODS AND MATERIALS

The MRI scanner

A 0.23-Tesla open MRI scanner (Philips Medical Systems, Cleveland, OH) was used for this study. The MRI scanner consists of two poles approximately 1 m in diameter each. The separation between the two poles is 47 cm. The MRI scan table can be moved in orthogonal planes along a set of rails mounted on the floor and on an orthogonal set of rails built in the couch. Vertical adjustment can be accomplished using a composite flat top with hard foam spacers beneath the patient. A set of three triangulation lasers (center and laterals) identical to those used on linear accelerators has been used for patient positioning.

CT and MR imaging procedure

Patients were scanned on a CT simulator (PICKER PQ 5000, Philips Medical Systems, Cleveland, OH) with a field of view (FOV) of 480 mm, 512 × 512 matrix (spatial resolution 0.94 mm), and a slice thickness of 3 mm. The axial CT slices extended from the third lumbar vertebrae to the middle of the femurs. Patients were advised to have a full bladder and were scanned in a supine position in a customized alpha cradle with knee support and a foot holder. Three steel ball fiducials (1 mm in diameter) were used (one anterior and two laterals) on the skin surface to mark the center of the prostate as an isocentric slice. Skin tattoos corresponding to these fiducial markers were aligned for daily treatment set up. The CT data were transferred to the treatment planning workstation and the patient was transferred to the MRI room for scanning usually within 0.5 h after CT.

Patients were MRI-scanned in a supine position in an alpha cradle with knee support and a foot holder (the same as for CT). Three donut-shaped fiducials (IZI Medical Products, Inc., Baltimore, MD) were superimposed on the tattoos that mark the center of the prostate as indicated by CT. In this position, MRI landmarks were made. One axial reference image was obtained. A sagittal image was obtained through the center of the prostate as depicted on the axial image. A series of 48 axial slices covering the whole pelvis based on the sagittal image was acquired. The T2-weighted turbo spin echo, three-dimensional sequence was performed for this study. Detailed parameters are repetitive time/echo time (TR/TE) = 3000/140 ms, FOV = 450–500 cm (de-

pending on patients' anatomic dimensions), matrix = 256 × 256 (spatial resolution 1.76–1.95 mm), echo train length (ETL) = 32, Flip angle = 90°, slice thickness = 3 mm, number of excitations (NEX) = 1, bandwidth (BW) = 39.5 kHz with horizontal frequency direction, and 9-min scan time. The magnetic resonance images were postprocessed for image distortion correction using the GDC software. The distortion-corrected MRIs were transferred to the treatment planning workstation.

Target and structure delineation

In our institution, CT-MRI fusion with CT-based dose calculation has been a routine procedure for all prostate cancer patients. Each patient underwent a CT and MRI scan as part of a routine simulation procedure. CT and MRIs (after GDC) were fused according to bony anatomy using either chamfer matching or maximization of mutual information methods. These fusion methods are available in the AcQSim system (Philips Medical Systems) used for this work. After image fusion, an evaluation of the fusion was performed. The results were checked by contouring bony landmarks on a minimum of three different slices: the central slice of the prostate and a few slices superior and inferior to the central slice. Our criterion for acceptance of the fusion was that the contours of the bones matched to within 2 mm on all three slices. Fifteen patients' CT and MRI data were used for this study.

In our clinical routine fusion procedure, the CT images were loaded first as the primary image and the MRIs were loaded as the secondary image. The external contour was obtained using an automatic threshold program and the femoral heads were manually contoured based on the CT image. The targets and critical structures were delineated based on the MRIs by oncologists. All the contours either based on primary CT or on secondary MRI were saved on the primary CT data set and were used for CT-based treatment planning. For MRI-based treatment planning, we loaded the MRIs as the primary image and the CT as the secondary image. The external contours were generated directly on the MRI data. The same internal contours as used in CT-based treatment planning were used for MRI-based treatment planning by manually copying target and critical structure contours from CT to MRI according to the color wash images of these structures. This is a feature available on the AcQSim system when a previous primary image is reloaded as a secondary image (direct contour transfer from a primary image to a secondary image is not possible). Although manually transferring internal contours could introduce some small errors, it was considered to be more reliable to use the same internal structure contours for our plan comparison than using new contours generated independently on MRI because this would introduce additional and potentially more significant uncertainties in the contours between MRI-based and CT-based treatment planning.

Table 1. Patient lateral dimensions measured on CT (distortion-free) and the residual distortions on MRI calculated as the difference between external contour points along the lateral axis on the isocentric slice on CT and those on GDC-corrected MRI

No. of patients	Patient sizes (cm)	Maximum residual distortion (cm)
2	<36.0	0.2 (0.0–0.2)
5	36.0–38.0	0.7 (0.0–0.7)
4	38.5–40.0	1.0 (0.2–1.0)
4	>40.0	2.7 (0.3–2.7)

Abbreviations: CT = computed tomography; MRI = magnetic resonance imaging; GDC = gradient distortion correction.

Dose calculation and plan comparison

All the CT-based treatment plans were approved by oncologists according to our clinical criteria (see the following section) and were subsequently used for the treatment. The MRI-based IMRT plans were generated, only for plan comparison, using the same planning parameters as for CT-based planning in terms of the prescribed dose, fractions, beam energy, beam angles, dose constraints, and optimization parameters. We used 6-, 10-, and 18-MV photon beams and six to nine gantry angles/ports depending on patient's body geometry.

Paired plans were compared based on our clinical acceptance criteria for prostate IMRT at Fox Chase Cancer Center. The maximum dose must be lower than 120% of the prescribed dose. The 95% of the planning target volume (PTV) must receive ≥100% of the prescribed dose (D95). The volume of rectum receiving 40 Gy (V40) and 65 Gy (V65) must be ≤35% and ≤17%, respectively. For bladder, no well-defined criteria have been identified. As a consequence, we have initiated soft constraints such that V40 and V65 must be ≤50% and ≤25%, respectively. These constraints serve as a guide for treatment planning. There were many plans that did not meet the constraints because the bladder was not sufficiently full during simulation. For femoral heads, less than 10% of the volume (V10) should receive 50 Gy. The isodose distributions were examined on a slice-by-slice basis. Our acceptable range was that the minimum distance from the posterior edge of the prostate clinical target volume (CTV) to the prescription isodose line was 4 mm to 8 mm. No more than one slice was allowed to be <4 mm. The PTV is 8 mm larger than the CTV in all other directions. Additionally, the 90% isodose line must not encompass the half width of the rectum or the 50% isodose line must not encompass the full width of the rectum on any slice except in some cases in which the rectal volume was very small (27).

RESULTS

Measurement of target and structure volumes on CT and MRI

After a patient was scanned with MRI, the images were processed using the vendor provided GDC software. The

Table 2. Structure volumes (in cm^3) measured on MRI and on CT as reported by the Corvus system

Patient no.	GTV		SV		Rectum		Bladder	
	MRI	CT	MRI	CT	MRI	CT	MRI	CT
1	34	33	6	5	94	91	93	91
2	35	33	NA	NA	79	76	124	122
3	62	60	NA	NA	48	46	124	122
4	57	55	11	11	70	68	78	76
5	93	92	15	16	118	116	64	63
6	135	132	5	6	95	92	116	113
7	68	66	5	5	55	51	168	165
8	64	63	8	8	42	44	195	192
9	55	54	4	4	55	53	274	269
10	47	45	10	10	51	49	209	208
11	31	31	6	6	38	37	56	57
12	30	29	3	3	63	61	164	162
13	36	36	5	5	55	52	168	166
14	60	60	12	12	50	49	87	88
15	67	66	9	9	51	49	103	102

Abbreviations: MRI = magnetic resonance imaging; CT = computed tomography; GTV = gross tumor volume; SV = seminal vesicle.

MRI distortion was reduced significantly after the GDC. Table 1 summarizes the relationship between patient's anatomic size and the residual distortion error after GDC along the lateral axis on the isocenter slice. The residual error was within 1 cm for patients with lateral dimensions <40 cm.

An additional uncertainty in the dose–volume histogram (DVH) comparison (see the following section) between CT- and MRI-based treatment planning is the difference in the target and structure contours resulting from manual transfer from the CT data sets to the MRI data sets. Table 2 shows the values of the structure volumes measured on MRI and on CT on the Corvus system. The volumes of the GTV from MRI are consistently slightly greater than those measured from CT. The maximum differences of the GTV between the two data sets are 6% (2 cc in absolute volume), 20% (1 cc in absolute volume) on seminal vesicles (SVs) (range, 17–20%), 8% (4 cc in absolute volume) on rectums (range, 2–8%), and 3% (2 to 3 cc in absolute volume) on bladders (range, 0.5–3%). Small changes in contour volumes were also observed between the CT and MR images after they were transferred from the AcQSim system to the Corvus system. The volumes measured on Corvus were smaller than those from the AcQSim by up to 6%. Table 3 compares the ratios of the MRI volumes with the CT volumes between AcQSim and Corvus.

These small volume discrepancies between the two data sets were thought to be due to the image resolution and algorithmic differences in volume determination in the AcQSim software and the Corvus system, and to the uncertainties introduced by the manual transfer of the contours between the two data sets.

Table 3. Ratios of structure volumes shown on MRI and those shown on CT as reported by AcQSim and Corvus

Patient no.	GTV		SV		Rectum		Bladder	
	AcQSim	Corvus	AcQSim	Corvus	AcQSim	Corvus	AcQSim	Corvus
1	1.07	1.03	1.07	1.20	1.08	1.03	1.04	1.02
2	1.06	1.06	N/A	N/A	1.07	1.04	1.05	1.02
3	1.04	1.03	N/A	N/A	1.03	1.04	1.03	1.02
4	1.05	1.04	1.06	1.0	1.04	1.03	1.04	1.03
5	1.04	1.01	1.04	0.94	1.05	1.02	1.05	1.02
6	1.04	1.02	1.03	0.83	1.05	1.03	1.05	1.03
7	1.05	1.03	1.07	1.00	1.04	1.08	1.04	1.02
8	1.04	1.02	1.06	1.00	1.03	0.95	1.03	1.02
9	1.05	1.02	1.02	1.00	1.03	1.04	1.03	1.02
10	1.05	1.04	1.05	1.00	1.03	1.04	1.03	1.00
11	1.06	1.00	1.03	1.00	1.05	1.03	1.05	0.98
12	1.05	1.03	1.00	1.00	1.05	1.03	1.02	1.01
13	1.04	1.00	1.02	1.00	1.08	1.06	1.03	1.01
14	1.03	1.00	1.05	1.00	1.08	1.02	1.02	0.99
15	1.04	1.02	1.05	1.00	1.08	1.04	1.03	1.01

Abbreviations as in Table 2.

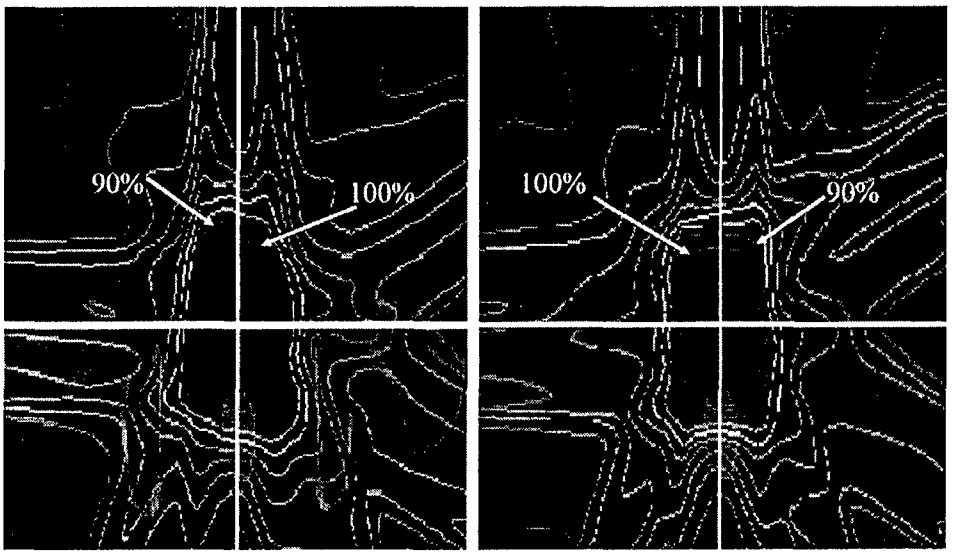

(a)

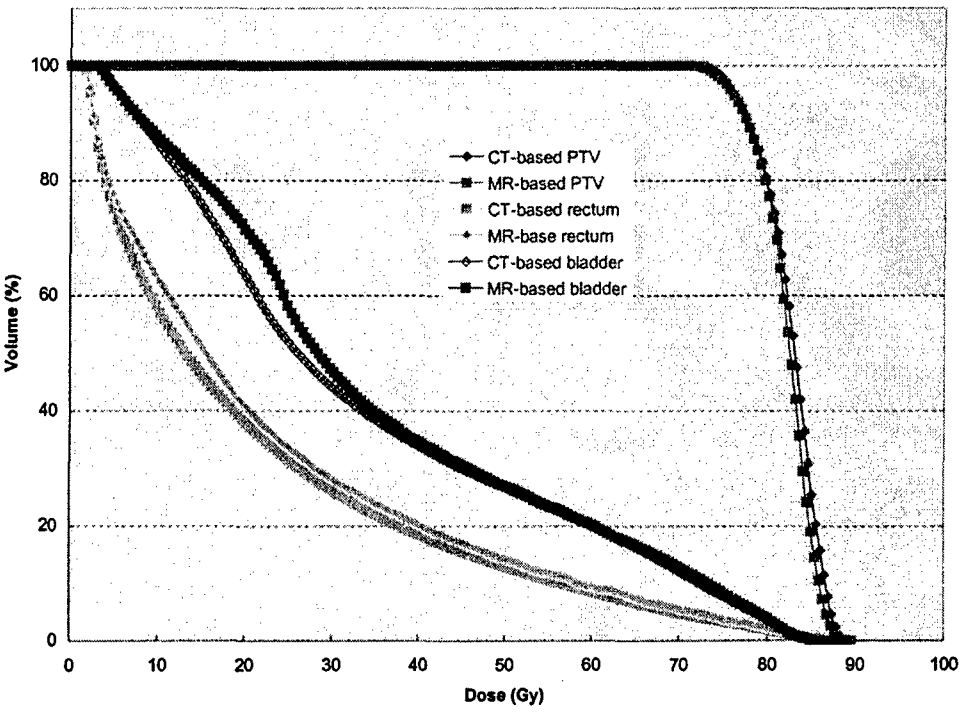

(b)

Fig. 1. Comparison of isodose distributions (a) and dose–volume histograms (b) for planning target volume, rectum, and bladder between computed tomography–based and magnetic resonance imaging–based intensity-modulated radiation therapy plans. The isodose lines are 100%, 90%, 80%, 70%, 60%, 50%, 40%, 30%, 20%, and 10%, respectively.

These differences may have small effects on the DVH comparison between MRI and CT in this work (see the following section). However, this effect will not be a problem when contours are drawn directly on MRI for MRI-based treatment planning in the future.

Comparison of CT- and MR-based treatment plans

Figure 1a shows an example of isodose distributions of IMRT plans based on CT and MRI. The data were taken from Patient 1. It can be seen that the 2 plans look very similar in terms of isodose distributions and they are all

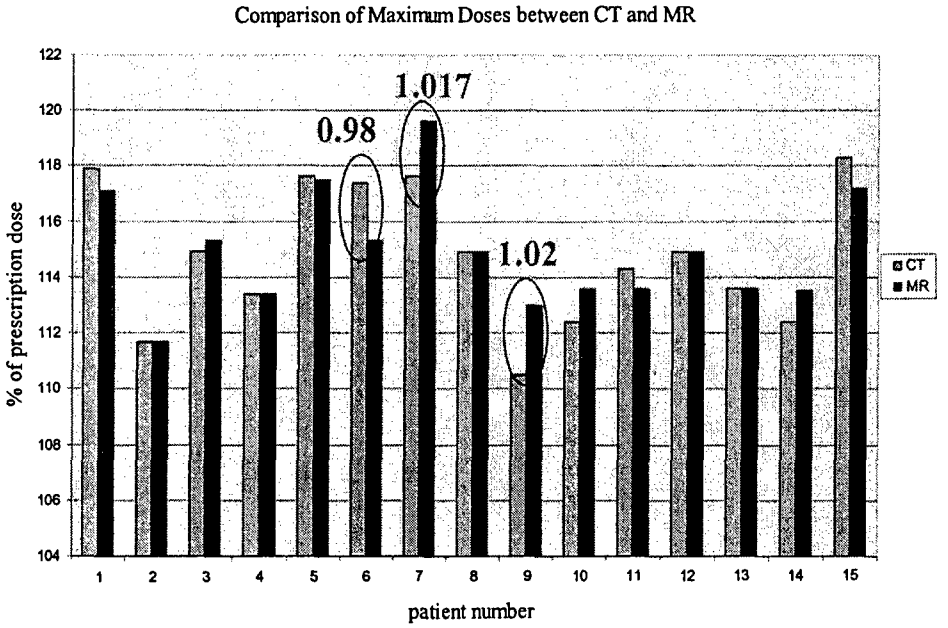

Fig. 2. Comparison of the maximum doses between computed tomography–based and magnetic resonance imaging–based intensity-modulated radiation therapy plans.

acceptable according to our clinical criteria. Figure 1b further compares the DVHs from the CT-based and MRI-based IMRT plans for the same patient. Again the differences are clinically insignificant. The differences for the bladder partially are due to the small differences in the structure volumes between the two image modalities. Because of the voxel size difference between MRI and CT, the bladder volumes may differ by 7% in some cases. As we have mentioned previously, this effect will no longer be a problem when we perform contouring and treatment planning on MRI directly.

Maximum doses

Figure 2 shows the maximum doses between CT- and MRI-based plans. Our clinical criterion for maximum dose

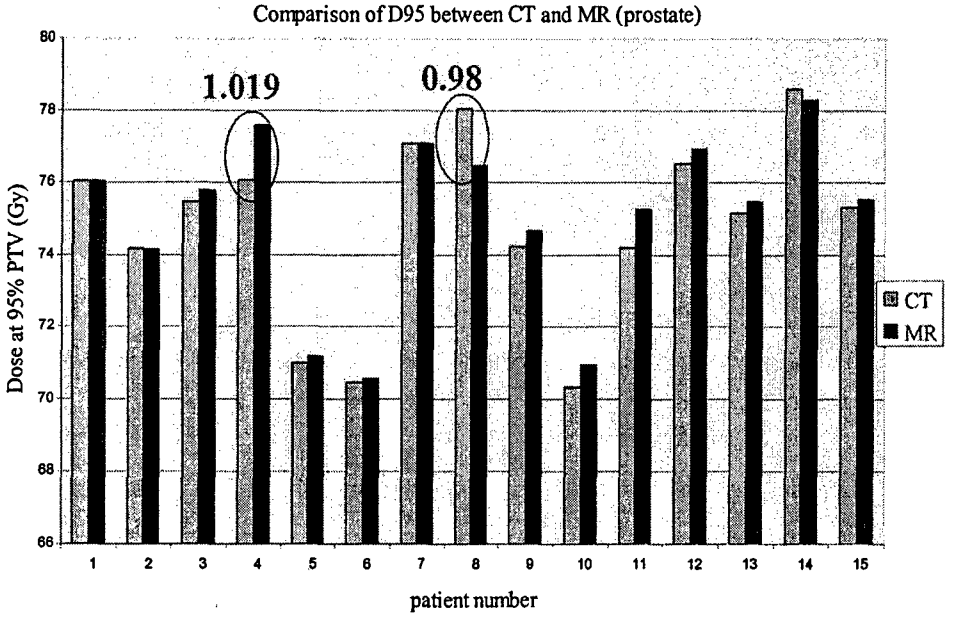

Fig. 3. Comparison of the planning target volume doses between computed tomography–based and magnetic resonance imaging–based intensity-modulated radiation therapy plans.

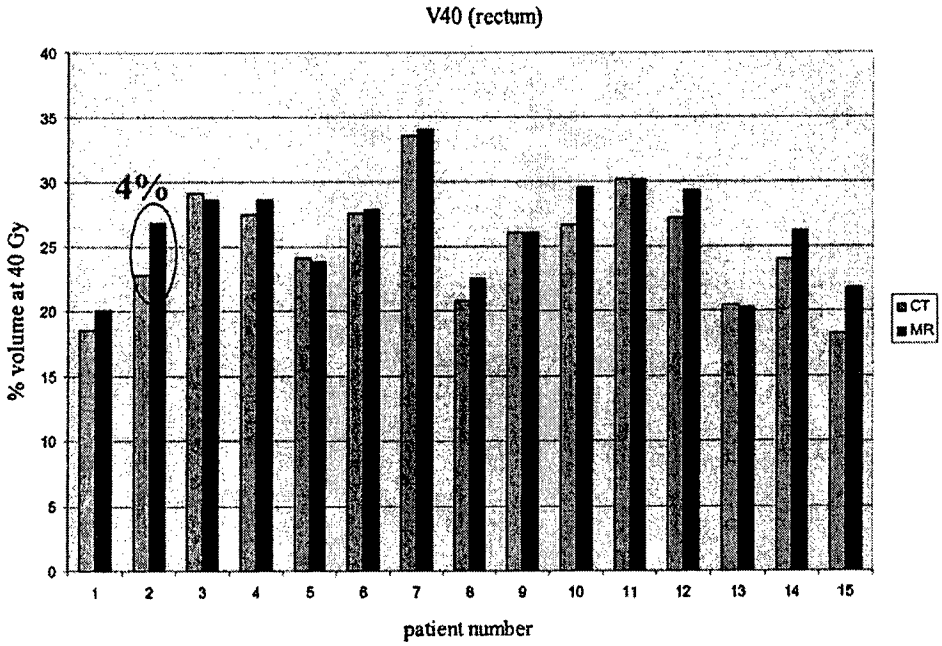

(a)

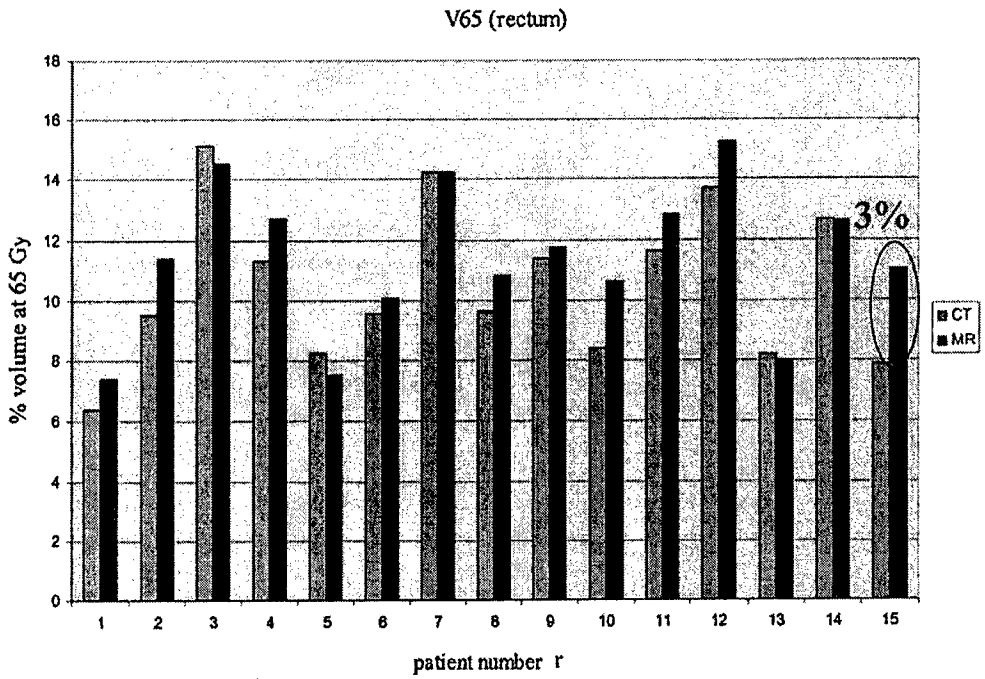

(b)

Fig. 4. Comparison of V40 (a) and V65 (b) of the rectum between computed tomography–based and magnetic resonance imaging–based intensity-modulated radiation therapy plans.

is below 120% of the prescription dose. Our results showed that the maximum doses were within 120% for all 15 patients and the dose differences between the CT-based and MRI-based plans were within 2%.

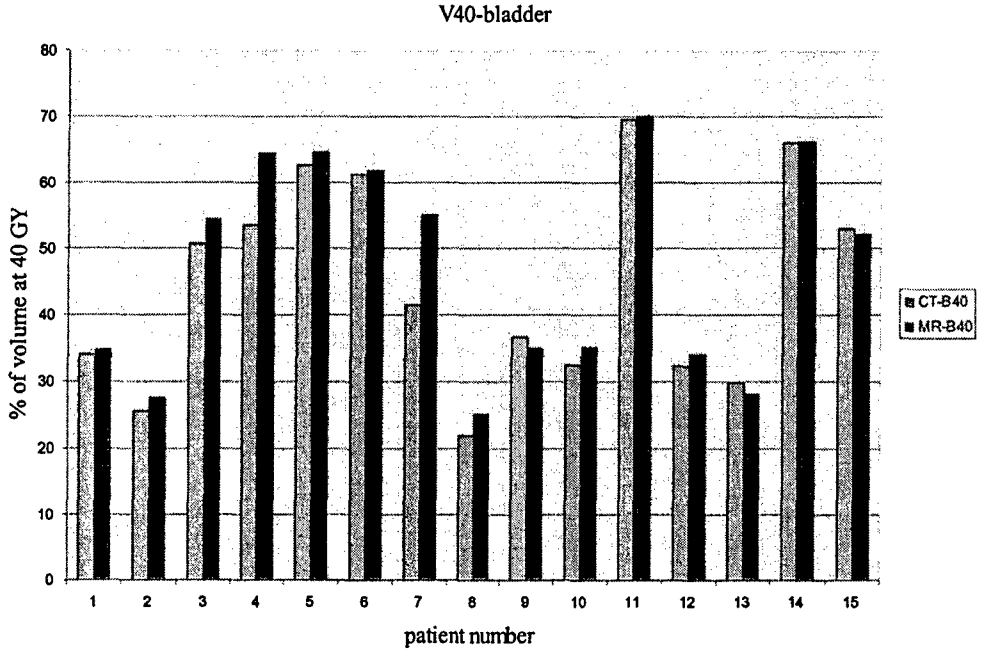

(a)

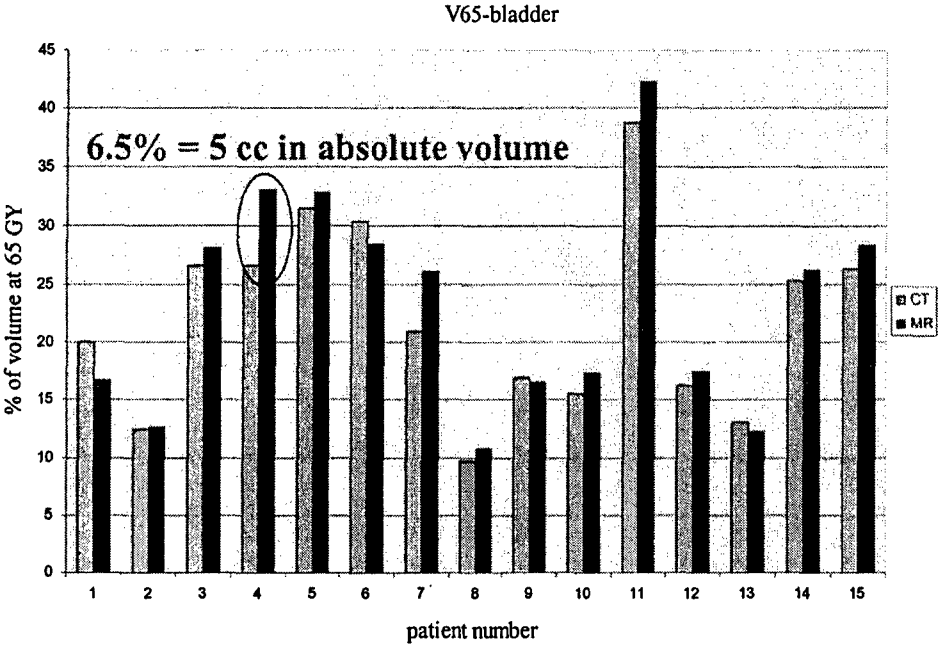

(b)

Fig. 5. Comparison of V40 (a) and V65 (b) of the bladder between computed tomography–based and magnetic resonance imaging–based intensity-modulated radiation therapy plans.

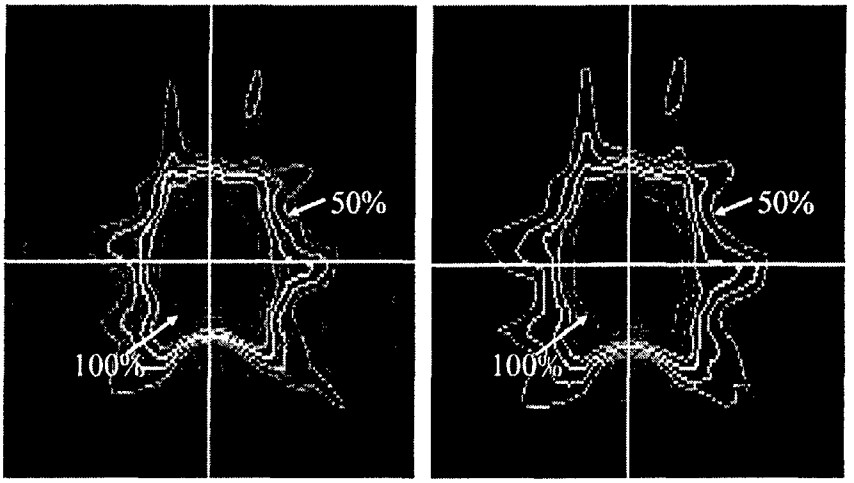

(a)

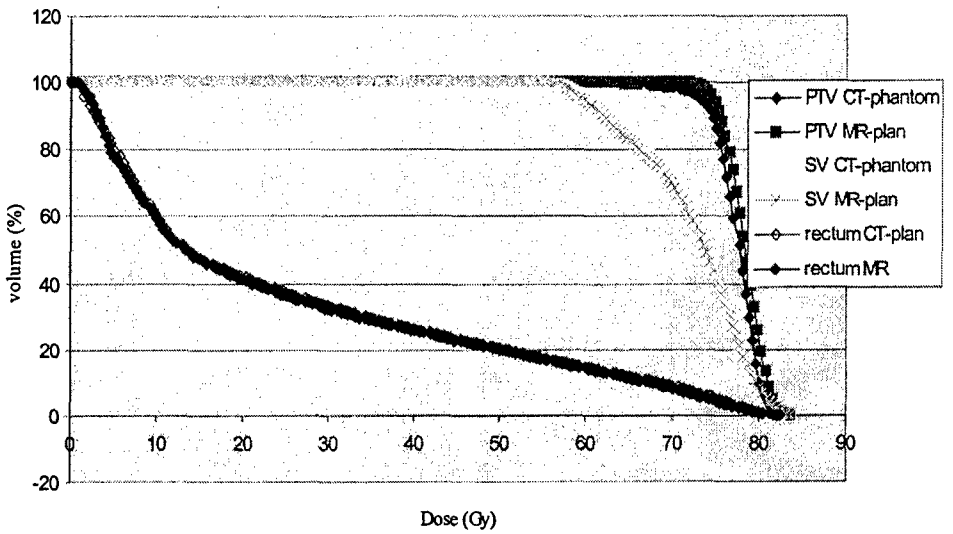

(b)

Fig. 6. Isodose distributions of a magnetic resonance imaging–based treatment plan and the plan recomputed using patient computed tomography data (a) and the corresponding dose–volume histograms for the planning target volume, seminal vesicles, and the rectum (b). The isodose lines are 100%, 90%, 80%, 70%, 60%, and 50%, respectively.

PTV doses

We have compared DVHs for prostate PTV using D95. Figure 3 shows the D95 values from CT-based plans and MRI-based plans for the 15 patients investigated. The largest difference in dose coverage between the two plans was 2% of the prescription dose for Patient 8.

Rectal doses

Figure 4 gives V40 and V65 values for the rectum. As can be seen from Fig. 4a, the largest difference in V40 is 4% (= 3 cc in absolute volume) for Patient 2, whose rectal volumes differed by 4% (3 cc in absolute volume) between CT and MRI as shown in Table 2. The differences in V65 were all within 3% between CT-based and MRI-based plans as seen in Fig. 4b. All the V40 and V65 values meet our clinical acceptance criterion.

Bladder doses

Figure 5 shows the V40 and V65 values for the bladder. Again, the differences between CT-based and MRI-based treatment plans are clinically acceptable. The maximum difference is 6.5% (= 5 cc absolute volume) in V65 for Patient 4 (Fig. 5b), which can be partially attributed to the 3% (2 cc in absolute volume) uncertainty of the contours between CT and MRI.

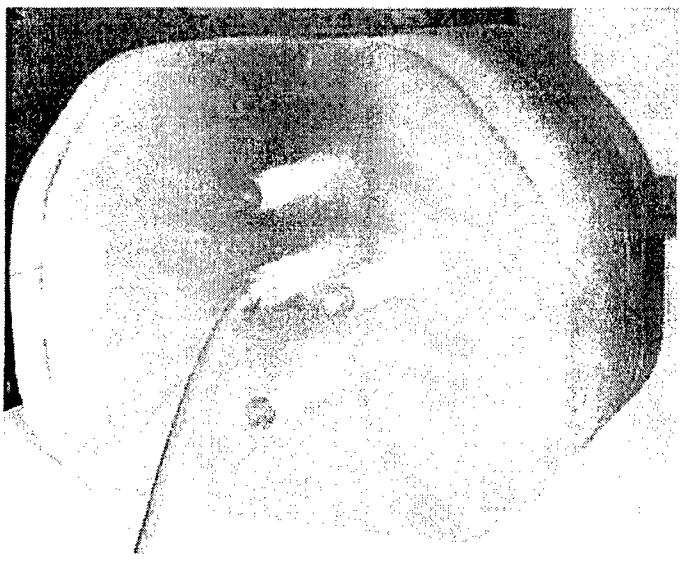

(a)

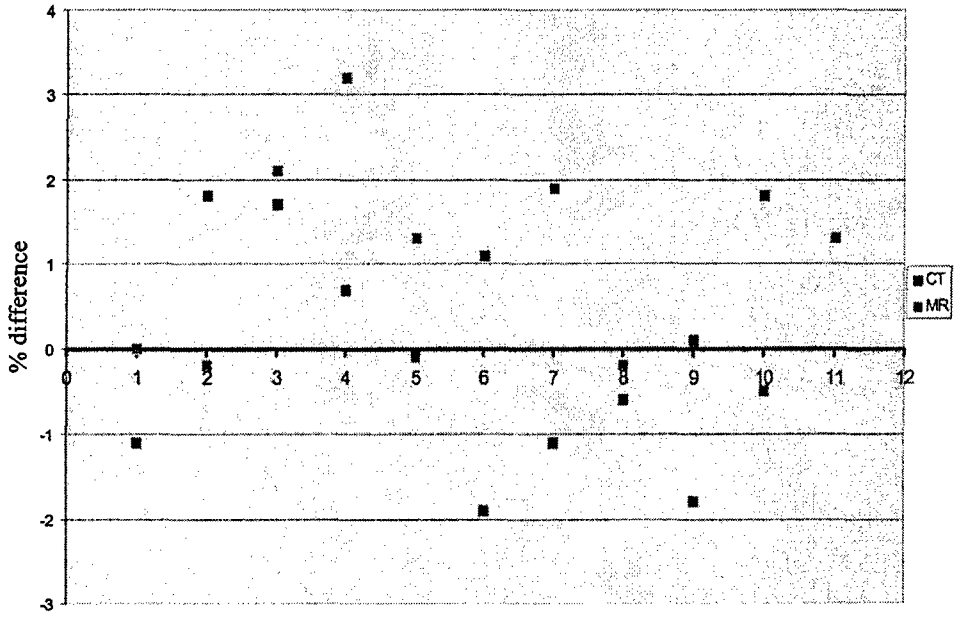

(b)

Fig. 7. An intensity-modulated radiation therapy (IMRT) quality assurance (QA) phantom used for this study (a) and the percent differences in isocenter doses between computed tomography–based and magnetic resonance imaging–based IMRT plans measured using the QA phantom.

Quality assurance for IMRT

To validate the dosimetric accuracy of MRI-based treatment planning, we have recomputed the patient dose distributions using the patient CT data and the MLC leaf sequences generated from the MRI-based patient IMRT plans. Figure 6a shows the isodose distributions of the IMRT plan generated based on MRI data and that recomputed based on CT data, and Fig. 6b shows the DVHs of the PTVs and the rectum for the two plans. The differences in dose are generally smaller than 2% of the prescription dose (or within 2 mm of isodose shift). Small differences in DVH were found because of the differences in structure volumes between CT and MRI. These small differences are considered to be clinically insignificant.

We also performed measurements on a quality assurance (QA) phantom to verify Monitor Unit (MU) calculations for

MRI based treatment planning. Figure 7a shows the QA phantom we used routinely for IMRT dosimetry verification. The hybrid plans were generated for both the CT-based plans and the MRI-based plans using the leaf sequences and associated MU designed for the corresponding patient plans. The physical phantom was irradiated using the same leaf sequences to verify the dosimetric accuracy of the treatment plans. The MRI-based MU calculation is accurate in comparison with measurements as shown in Fig. 7b. The largest difference of 3.2% between MRI-based dose calculation and measurements was seen on Patient 4. Figure 7b also clearly demonstrated that MUs calculated based on MRI and those calculated based on CT are consistent.

DISCUSSION

Effect of MRI distortions on dose calculation

At our institution, we have clinically implemented MRI-based treatment planning for prostate IMRT. To ensure the dosimetry accuracy of MRI-based treatment planning, we selected patients with maximum lateral dimensions $\leq$38 cm. For patient lateral sizes larger than 38 cm we use the CT and MRI fusion technique with CT-based dose calculation. For 6 weeks, we measured lateral dimensions for all the new prostate IMRT patients and found that 41 of 46 (89%) patients were $\leq$38 cm, 4 of 46 (9%) were 39–39.5 cm, and only 1 (2%) patient was greater than 40 cm in lateral dimensions. As shown in Table 1, the GDC software worked well for patient sizes less than 38 cm with residual distortion errors less than 7 mm.

In this study, we have demonstrated that with GDC, MRI-based treatment planning is adequate for prostate IMRT using the Corvus inverse planning system. The residual MRI distortions did not seem to affect IMRT dose calculations, because most differences in the external contours along the major axes were less than 1 cm. The difference could be more than 1 cm in other directions off the major axes and the effect could be greater if a beam was incident in those directions. However, when multiple beams were used in an IMRT treatment, it is unlikely that a treatment plan will be affected significantly if only one or two beams will be affected by 1–2 cm differences in the external contours of the patient.

Our results showed that the difference between CT-based and MRI-based treatment planning for maximum target doses is less than 2%, and for D95 of the prostate is also within 2%. The differences in V40 and V65 for the rectum are within 4%. The largest discrepancies of V40 and V65 for the bladder were seen on Patients 4 and 7, which did not correspond to the largest residual distortions appeared on Patients 1, 5, 6, and 8 with lateral dimensions greater than 40 cm. The dose discrepancies on V40 and V65 of the bladder were believed to be caused by the small volume discrepancies between the two imaging modalities as well as the uncertainties introduced by manually transferring the contours from CT to MRI. However, these differences will no longer be a problem when MRI alone is used for treatment planning.

Creating MR-based DRR for patient setup

Digitally reconstructed radiographs (DRRs) from patient CT data are routinely used for patient initial setup verification by comparing with images taken using portal film or electronic portal imaging devices. However, MRI-derived DRRs do not provide bony structure information and therefore cannot be used directly for checking patient positions. To overcome this problem, relevant bony structures including pubic symphysis, acetabulum, femoral heads and sacrum were contoured using AcQSim and assigned a bulk density of 2.0 g/cm^3. The bony structures were then clearly shown on the MRI-derived DRRs, which could be used for patient initial setup verification by comparing with portal films. The accuracy of this method was verified by comparing with CT-derived DRRs (within 2–4 mm) based on our contour experiences on MRI. The BAT (B-mode Acquisition and Targeting, NOMOS Corp.) ultrasound system is also used for daily target localization to correct for prostate interfraction motion. The BAT ultrasound images agreed better with MRI-generated soft-tissue contours than CT-generated contours.

CONCLUSIONS

This article investigates MRI-based treatment planning for IMRT of prostate cancer. We summarize the results and conclusions of this investigation as follows.

1. We investigated the effect of MRI residual distortion after GDC on IMRT treatment planning and dosimetry accuracy. The residual distortion errors are less than 1 cm and will have negligible clinical impact for more than 90% of the prostate patients whose lateral dimensions are <40 cm.
2. We also studied structure volume differences between CT and MRI on the AcQSim and Corvus systems, which led to small discrepancies in DVH curves for those structures with significant differences. These differences reflected the inherent uncertainties of target and structure delineation using different imaging modalities and different treatment planning systems. However, these DVH discrepancies will not be a problem when MRI alone is used for treatment planning because both structure contouring and treatment optimization will be performed using the same imaging modality.
3. We evaluated MRI- and CT-based IMRT treatment optimization for plan consistency. Because both planning techniques will be used clinically and in different treatment protocols, it is essential to ensure IMRT plans using both imaging modalities are consistent in terms of target coverage, dose conformity, and normal tissue sparing. Our results showed that no clinically significant differences were found between MRI- and CT-based treatment plans using the same beam arrangements, dose constraints, and optimization parameters.
4. We validated the dosimetry accuracy of MRI-based treatment planning by recomputing MRI-based IMRT

plans using patient CT data and an IMRT QA phantom. The differences in dose distributions between MRI plans and the corresponding recomputed plans were generally within 3%/3 mm. The differences in isocenter doses between MRI dose calculation and phantom measurements were within our clinical criterion of 4%.

5. To facilitate initial patient setup, MRI-based DRRs were generated, which included structure outlines for relevant bony landmarks such as pubic symphysis, acetabulum, femoral heads, and sacrum. The BAT ultrasound system was used to localize the treatment target for prostate IMRT.

REFERENCES

1. Schellhammer PF, el Mahdi AM, Higgins EM, *et al.* Prostate biopsy after definitive treatment by interstitial 125 iodine implant or external beam radiation therapy. *J Urol* 1987;137: 897–901.
2. Zelefsky MJ, Leibel SA, Gaudin PB, *et al.* Dose escalation with three-dimensional conformal radiation therapy affects the outcome in prostate cancer. *Int J Radiat Oncol Biol Phys* 1998;41:491–500.
3. Hanks GE, Hanlon AL, Schultheiss TE, *et al.* Dose escalation with 3D conformal treatment: Five year outcomes, treatment optimization and future directions. *Int J Radiat Oncol Biol Phys* 1998;41:501–510.
4. Hanks GE. Progress in 3D conformal radiation treatment of prostate cancer. *Acta Oncol* 1999;38(Suppl. 13):69–74.
5. Pollack A, Zagars GK, Rosen II. Prostate cancer treatment with radiotherapy: maturing methods that minimize morbidity. *Semin Oncol* 1999;26:150–161.
6. Pollack A, Zagars GK, Smith LG, *et al.* Preliminary results of a randomized radiotherapy dose-escalation study comparing 70 Gy with 78 Gy for prostate cancer. *Jof Clinical Oncology* 2000;18:3304–3911.
7. Pollack A, Zagars GK, Starkschall G, *et al.* Prostate cancer radiation dose response: Results of the M. D. Anderson phase III randomized trial. *Int J Radiat Oncol Biol Phys* 2002;53: 1097–1105.
8. Yeoh EEK, Fraser RJ, McGowan RE, *et al.* Evidence for efficacy without increased toxicity of hypofractionated radiotherapy for prostate carcinoma: Early results of a Phase III randomized trial. *Int J Radiat Oncol Biol Phys* 2003;55:943–955.
9. Khoo VS, Adams EJ, Saran F, *et al.* A comparison of clinical target volumes determined by CT and MRI for the radiotherapy planning of base of skull meningiomas. *Int J Radiat Oncol Biol Phys* 2000;46:1309–1317.
10. Tanner SF, Finnigan DJ, Khoo VS, *et al.* Radiotherapy planning of the pelvis using distortion corrected MR images: The removal of system distortions. *Phys Med Biol* 2000;45:2117–2132.
11. Potter R, Heil B, Schneider L, *et al.* Sagittal and coronal planes from MRI for treatment planning in tumors of brain, head and neck: MRI assisted simulation. *Radiother Oncol* 1992;23:127–130.
12. Rasch C, Barillot I, Remeijer P, *et al.* Definition of the prostate in CT and MRI: A multi-observer study. *Int J Radiat Oncol Biol Phys* 1999;43:57–66.
13. Krempien RC, Schubert K, Zierhut D, *et al.* Open low-field magnetic resonance imaging in radiation therapy treatment planning. *Int J Radiat Oncol Biol Phys* 2002;53:1350–1360.
14. Debois M, Oyen R, Maes F, *et al.* The contribution of magnetic resonance imaging to the three-dimensional treatment planning of localized prostate cancer. *Int J Radiat Oncol Biol Phys* 1999;45:857–865.
15. Chen L, Price R, Li J, *et al.* Evaluation of MRI-based treatment planning for prostate cancer using the AcQplan system [Abstract]. *Med Phys* 2003;30:1507.
16. Beavis AW, Gibbs P, Dealey RA, *et al.* Radiotherapy treatment planning of brain tumours using MRI alone. *Br J Radiol* 1998;71:544–548.
17. Guo WY. Application of MR in stereotactic radiosurgery. *J Magn Res Imag* 1998;8:415–420.
18. Mah D, Michael S, Hanlon A, *et al.* MRI simulation: Effect of gradient distortions on three-dimensional prostate cancer plans. *Int J Radiat Oncol Biol Phys* 2002;53:757–765.
19. Mah D, Steckner M, Palacio E, *et al.* Characteristics and quality assurance of a dedicated open 0.23 T MRI for radiation therapy simulation. *Med Phys* 2002;29:2541–2547.
20. Michiels J, Bosmans H, Pelgrims P, *et al.* On the problem of geometric distortion in magnetic resonance images for stereotactic neurosurgery. *Magn Res Imag* 1994;12:749–765.
21. Mizowaki T, Nagata Y, Okajima K, *et al.* Reproducibility of geometric distortion in magnetic resonance imaging based on phantom studies. *Radiother & Oncol* 2000;57:237–242.
22. Lee YK, Bollet M, Charles-Edwards G, *et al.* Radiotherapy treatment planning of prostate cancer using magnetic resonance imaging alone. *Radiother & Oncol* 2003;2:203–216.
23. Ma C-M, Mok E, Kapur A, *et al.* Clinical implementation of a Monte Carlo treatment planning system. *Med Phys* 1999;26: 2133–2143.
24. Ma C-M, Pawlicki T, Jiang SB, *et al.* Monte Carlo verification of IMRT dose distributions from a commercial treatment planning optimization system. *Phys Med Biol* 2000;45:2483–2495.
25. Chen L, Li J, Mah D, *et al.* Monte Carlo investigation of dosimetry accuracy for MR-based treatment planning [Abstract]. *Med Phys* 2002;29:1339.
26. Fransson A, Andreo P, Potter R. Aspects of MR image distortions in radiotherapy treatment planning. *Strahlenther Onkol* 2002;177:59–73.
27. Pollack A, Price RA. IMRT for prostate cancer. In: Palta JR, Mackie TR, editors. Intensity-modulated radiation therapy: The state of the art. AAPM Monograph No. 29. WI. Medical Physics Publishing, Madison; 2003. pp. 617–630.